The Canadian Mineralogist
Vol. 39, pp. 831-853 (2001)

COMPOSITIONAL TRENDS IN Fe, Co AND Ni SULFARSENIDES AND THEIR CRYSTAL-CHEMICAL IMPLICATIONS: RESULTS FROM THE ARROYO DE LA CUEVA DEPOSITS, RONDA PERIDOTITE, SOUTHERN SPAIN

SKAGE R. HEM[§] AND EMIL MAKOVICKY

Department of Mineralogy, Geological Institute, University of Copenhagen, Østervoldgade 10, DK–1350 Copenhagen, Denmark

FERNANDO GERVILLA

Instituto Andaluz de Ciencias de la Tierra y Departamento de Mineralogía y Petrología, Facultad de Ciencias, C.S.I.C. – Universidad de Granada, E–18002 Granada, Spain

ABSTRACT

Fe–Co–Ni sulfarsenides and diarsenides in a pyrrhotite matrix were found as localized segregations in the Arroyo de la Cueva area, at the northwestern margin of the Ronda Peridotite. The pyrrhotite matrix encloses alloclasite, löllingite and pentlandite, and is cross-cut by veins of chalcopyrite–cubanite intergrowths hosting arsenopyrite, cobaltite and sphalerite, as well as chlorite–magnetite and calcite–talc with minor arsenopyrite and löllingite. Alloclasite, arsenopyrite, cobaltite, löllingite and pentlandite show strong variation in their contents of Fe, Co, Ni, As and S. Textural and chemical evidence suggests that the ore initially formed at high temperatures and low fugacities of sulfur. The ore was subsequently metasomatized at conditions of gradually increasing sulfur fugacity and decreasing temperatures. The variations in Fe, Co and Ni in alloclasite, cobaltite and pentlandite describe linear trends. These trends were compared with similar trends from other, especially mafic–ultramafic associations. They depend on both mineral association and the requirement that a structure-specific number of nonbonding metal *d* electrons be maintained. Three types of trends are shown by the sulfarsenides. 1) Trends describing Co replacement by a mixture of Fe and Ni are shown by sulfarsenides occurring in metal-rich environments. 2) Trends where Co is replaced by Ni occur in associations containing either pyrite, sulfarsenides or diarsenides indicative of higher anion fugacities. 3) Trends shown by sulfarsenides associated with skutterudite describe replacement of Ni by a mixture of Co and Fe. The trends defined by pentlandite compositions indicate the substitution Fe + Ni → 2 Co and support previously suggested bonding models.

Keywords: Fe–Co–Ni sulfarsenides, compositional trends, crystal chemistry, alloclasite, cobaltite, löllingite, pentlandite, pyrrhotite, smythite, Ronda Peridotite, Spain.

SOMMAIRE

Des sulfarséniures et diarséniures de Fe–Co–Ni sont présents dans une matrice de pyrrhotite en ségrégations locales dans la région d'Arroyo de la Cueva, le long de la bordure nord-ouest de la péridotite de Ronda, en Espagne. Cette matrice renferme alloclasite, löllingite et pentlandite, et est recoupée par des veines de chalcopyrite–cubanite en intercroissance renfermant arsénopyrite, cobaltite et sphalérite, de même que chlorite–magnétite et calcite–talc, avec arsénopyrite et löllingite accessoires. Alloclasite, arsénopyrite, cobaltite, löllingite et pentlandite font preuve de variations importantes dans leur contenu de Fe, Co, Ni, As et S. D'après l'évidence texturale et chimique, le minerai s'est formé d'abord à température élevée et à faible fugacité en soufre. Par la suite, le minerai a subi une métasomatose au cours d'une augmentation graduelle de la fugacité du soufre et d'une diminution en température. Les variations en Fe, Co et Ni dans l'alloclasite, la cobaltite et la pentlandite sont linéaires. Ces tracés sont comparés aux résultats de suites semblables, en particulier de suites mafiques–ultramafiques. Ils dépendent à la fois de l'association de minéraux et des exigeances en nombre d'électrons *d* non impliqués dans les liaisons, tel qu'imposé par la structure. Trois types de tracés sont évidents dans les sulfarséniures. 1) Un tracé décrivant le remplacement du Co par un mélange de Fe + Ni caractérise les sulfarséniures de milieux riches en métaux. 2) Un tracé illustrant le remplacement de Co par Ni est la marque d'associations contenant pyrite, sulfarséniures ou diarséniures et indiquant une fugacité plus élevée des anions. 3) Les sulfarséniures associés à la skutterudite montrent un tracé décrivant le remplacement de Ni par un mélange de Co et de Fe. Les tracés décrivant la composition de la pentlandite indiquent la substitution Fe + Ni → 2 Co et concordent avec les modèles de liaisons proposés antérieurement.

(Traduit par la Rédaction)

Mots-clés: sulfarséniures de Fe–Co–Ni, tracés de composition, chimie cristalline, alloclasite, cobaltite, löllingite, pentlandite, pyrrhotite, smythite, péridotite de Ronda, Espagne.

§ *E-mail address*: skage@geo.geol.ku.dk

Introduction

Ore accumulations in the Arroyo de la Cueva area, at the northwestern margin of the Ronda Peridotite, southern Spain, are localized around three abandoned mines. The Mina La Herrumbrosa is situated on the contact between the Ronda Peridotite and metamorphic rocks of the Cassares Unit, whereas the Mina San Pedro and the Mina Majar del Toro are both hosted by the Ronda Peridotite. The ore is dominated by pyrrhotite, chalcopyrite and cubanite. Local enrichments in Fe, Co, Ni, As, Bi and Au lead to the presence of alloclasite, arsenopyrite, cobaltite, löllingite, maldonite (Au_2Bi), pentlandite, and westerveldite, as well as native Au and Bi. The (Fe,Co,Ni)-sulfarsenides and pentlandite exhibit large variations in Fe, Co and Ni contents, and may even define distinct compositional trends. Similar compositional trends have been described in sulfarsenides (Béziat *et al.* 1996, Gervilla *et al.* 1998, Barkov *et al.* 1999) and pentlandite (Merkle & von Gruenewaldt 1986).

In previous investigations, theoretical and experimental studies of compositional variation in the disulfides, sulfarsenides and diarsenides of Fe, Co and Ni have led to bonding models and schemes of coupled substitution involving cations and anions. However, detailed analysis of the natural trends and a comparison of these with the crystal-chemical models have not been performed. Here, we systematically compare the predicted and the observed trends and their relation to the observed mineral associations.

Geological Background

The Ronda massif is a large body of ultramafic rocks hosted in the nappe complexes of the Betic Cordillera, which is part of the Rif–Betic orogeny. This massif of lherzolite and harzburgite represents a portion of lithospheric mantle emplaced at a high temperature in the continental crust, about 20–22 My ago (Priem *et al.* 1979, Zindler *et al.* 1983, Reisberg *et al.* 1989, Zeck *et al.* 1989). On the basis of its internal structure, the Ronda massif was affected by the infiltration of asthenospheric basaltic melts up to a certain level called the recrystallization front (Van der Wal & Bodinier 1996). Only small volumes of volatile-rich melt migrated upward past the recrystallization front, whereas below the recrystallization front, melt–rock reactions gave rise to variably recrystallized and depleted peridotites (Garrido & Bodinier 1999).

Three main types of mineralization have been recognized in the ultramafic massifs of the Rif–Betic orogeny (Gervilla & Leblanc 1990): chromite ores rich in interstitial Ni arsenides (Cr–Ni ores), Fe–Ni–Cu sulfide ores containing variable amounts of graphite (S–G ores), and interstitial Ni-arsenide-free magnesiochromite ores (Cr ores). The spatial distribution of these ore types correlates with the petrological zoning of the peridotite bodies, Cr–Ni and S–G ores being mainly encountered above the recrystallization front (Gervilla 1998).

The formation of Cr–Ni and S–G ores can be explained by the fractionation of small amounts of melt that migrated upward past the recrystallization front. The model involves a magma crystallizing chromite and pyroxene at elevated temperatures, leading to the saturation of arsenides and sulfides. The segregation of an immiscible arsenide–sulfide liquid ensued, which then developed into two liquids, a Ni-rich arsenide liquid and a Fe–Ni–Cu sulfide liquid (Gervilla *et al.* 1996). This mechanism separated the arsenide melt from the sulfide melt and led to the formation of Cr–Ni ores by the crystallization of Ni arsenides as a matrix around the chromite. The sulfide liquid subsequently formed the S–G ores.

The ores at Arroyo de la Cueva can be considered as evolved examples of S–G ores. They are found as thin veins and lenses located in joints and cracks cross-cutting the peridotite, which is heavily serpentinized in this area. The ore veins are surrounded by talc, chlorite and fibrous serpentine.

The mineral assemblage in S–G ores mainly consists of a matrix of Fe-rich pyrrhotite, enclosing grains of either cobaltian pentlandite or (Co,Ni)-rich löllingite and alloclasite. The pyrrhotite matrix commonly shows textures indicative of mechanical stress and deformation, such as disaggregation and lenticular zoning. These deformed aggregates are dominated by S-rich pyrrhotite. The pyrrhotite matrix is cross-cut by three different types of veins: 1) coarse intergrowths of chalcopyrite and cubanite associated with arsenopyrite, cobaltite and sphalerite, 2) chlorite and magnetite hosting minor löllingite and arsenopyrite, and 3) talc and calcite (with 2–5 at.% Mg). Metasomatism and deformation are common and have usually modified the original assemblage. Most pronounced is the replacement of pyrrhotite, löllingite and alloclasite by arsenopyrite and cobaltite, as well as the replacement of pyrrhotite and pentlandite by marcasite and violarite, respectively.

The primary ore-forming process is difficult to distinguish in the assemblages subjected to metasomatism and deformation, as both ore and host rock are tectonically reworked. One common denominator emerges from the data: the significant role played by hydrothermal solutions under decreasing temperature and rising sulfur fugacity. Apart from the primary paragenesis of pyrrhotite ± löllingite ± pentlandite ± alloclasite, none of the members of the complex mineral association can be attributed to magmatic processes. Studies of serpentine fibers and mineralized joints show a linkage between the late brittle tectonic regime and ore formation, arguing for a hydrothermal origin (Hem 1998).

The source of the fluid precipitating these phases is uncertain. Residual magmatic fluids that segregated after the formation of S–G ores could have migrated upward through the peridotite during the early stages of brittle deformation. The metasomatism could represent

the continued influence exercized by this fluid as it evolved, or it could have occurred during a separate episode linked to the serpentinization of the peridotite.

Crystal chemistry of MX_2 sulfides

From the point of view of polyhedra, the MX_2 minerals (M = Fe, Co, Ni or PGE, X = As, S or Sb) more or less follow the same structural and crystal-chemical principles. Table 1 summarizes the chemical composition, symmetry and general structure-type of the $(Fe,Co,Ni)(As,S)_2$ minerals. All of these structures contain tightly bonded anion pairs, in which each anion has tetrahedral coordination to one anion and three cations. The cations are octahedrally coordinated to six anions. Three different structure-types comprise the minerals of this group, the pyrite structure, the marcasite structure and the pararammelsbergite structure. The other structures in these groups can be viewed as derivatives of the above. The pararammelsbergite structure is transitional between the pyrite and the marcasite structures, in the sense that the cation coordination octahedra share corners in pyrite, one edge in pararammelsbergite, and two edges in marcasite. Order–disorder phenomena are of great importance at the anion sites and lead to diversity in the structures. Béziat *et al.* (1996) suggested that ordering of the metals controls the compositional trends that in some cases are exhibited by the sulfarsenides of Fe, Co and Ni.

TABLE 1. SUMMARY OF $M(X)_2$ MINERALS

Mineral	Ideal formula	General structure-type	Space group	Anion ordering	Ref.
Pyrite	FeS_2	Parent structure	*Pa*3	–	1
Cobaltite	CoAsS	Pyrite-type structure with various degrees of order among anions	*Pa*3	Disordered	2
			$Pca2_1$	Ordered	2
			$Pca2_1$	Ordered	3
			Pnnm	–	4
Gersdorffite	NiAsS	Pyrite-type structure with various degrees of order among anions and distortion	$P2_13$	Partial	5
			*Pa*3	Disordered	6
			*P*1	–	7
Pararammelsbergite	$NiAs_2$	Transitional between pyrite and marcasite	*Pbca*	–	8
Marcasite	FeS_2	Parent structure	*Pmnn*	–	9
Glaucodot	(Co,Fe)AsS	Marcasite	*Cmmm*	–	10
Alloclasite	CoAsS	Marcasite	$P12_11$	–	11
			$P22_12_1$	–	12
			Cmmm	–	13
Rammelsbergite	$NiAs_2$	Marcasite	*Pnnm*	–	14
Safflorite	$(Co,Fe)As_2$	Marcasite	*Pnnm*	–	15
Arsenopyrite	FeAsS	Modified marcasite. Fe atoms come together in pairs along *c*, causing periodic shortening of the *c* axis	$C112_1/d$	Partial	16
			$P12_1/c1$ and	–	
			*P*1	–	17
			$B12_1/d1$	–	18
Clinosafflorite	$CoAs_2$	Marcasite type, modified in the same way as arsenopyrite	*P*2/*n*	–	19
Löllingite	$FeAs_2$	Modified marcasite. Shortening of *c* axis	*Pnnm*	–	20

References: 1 Bragg (1914), 2 Giese & Kerr (1965), 3 Fleet & Burns (1990), 4 Polushkina & Sidorenko (1963), 5 Bayliss & Stephenson (1968), 6 Bayliss (1968a), 7 Bayliss (1968b), 8 Fleet (1972), 9 Buerger (1934), 10 Ferguson (1946), 11 Scott & Nowacki (1976), 12 Kingston (1971), 13 Berry & Thompson (1962), 14 Kaiman (1947), 15 Radcliffe & Berry (1968), 16 Fuess *et al.* (1987), 17 Morimoto & Clark (1961), 18 Buerger (1936), 19 Radcliffe & Berry (1971), 20 Buerger (1932).

Alloclasite and cobaltite are polymorphs of CoAsS, but significant amounts of Fe and Ni may substitute for Co, and As and S partly substitute for each other (Bayliss 1969, Klemm 1965, Petruk *et al.* 1971, Maurel & Picot 1974). Cobaltite is homeotypic with pyrite, Co taking the place of Fe, and AsS taking the place of S_2. Alloclasite is in a similar way derived from the marcasite structure, and the alloclasite–cobaltite relation is analogous to the marcasite–pyrite relation (Scott & Nowacki 1976). Two structural modifications of cobaltite have been reported, one with a disordered distribution of As–S pairs (cubic; Giese & Kerr 1965) and one with an ordered distribution (cubic; Giese & Kerr 1965; orthorhombic; Fleet & Burns 1990). The distribution of As and S is ordered in alloclasite (orthorhombic; Scott & Nowacki 1976).

The arsenopyrite (FeAsS) and löllingite ($FeAs_2$) structures are derivatives of the marcasite structure. In all these structures, the Fe coordination octahedra share edges perpendicular to the *c* axis. The *c* axis is gradually shortened when S is replaced by As. The arsenopyrite structure can therefore be viewed as an intermediate between the marcasite and the löllingite structures.

The structural modifications of the $(Fe,Co,Ni)(As,S)_2$ minerals can be listed according to increasing metal–metal interaction: pyrite – pararammelsbergite – marcasite – arsenopyrite – löllingite. Comparison of this structural variation with the compositions of the corresponding minerals led to the development of a set of models explaining the electronic configuration of MX_2 minerals. These models use crystal-field theory to explain the variation, producing an iso-electronic model (Hulliger 1968, Nickel 1968, Maurel & Picot 1974). This model explains each structure type as stabilized by a fixed number of nonbonding *d* electrons; pyrite ≥ 6, pararammelsbergite 6, marcasite 6, arsenopyrite 5 and löllingite 4. The *s* and *d* electrons of the metal are involved in covalent bonds with the anion groups, reducing the number of nonbonding *d* electrons as arsenic is introduced. The ideal valence of the cation is equal to the number of *s* and *d* electrons minus the nonbonding *d* electrons. This predicts valences of Fe^{2+}, Co^{3+} and Ni^{4+} in pyrite-type structures, such as cobaltite and gersdorffite, which are supported by the findings of Wood & Strens (1979). The anions correspondingly share two electrons within the anion group, thus giving these groups the formal valences of –2 for S_2, –3 for

AsS and –4 for As_2. A survey of the relevant stoichiometric phases and structures shows that they generally obey the iso-electronic model (Maurel & Picot 1974). This situation is complicated where the minerals deviate from stoichiometry and where coupled substitutions are required to maintain the required number of nonbonding *d* electrons. This model has been questioned by Tossell *et al.* (1981) and Tossell (1984), who concluded that anion–anion interaction is of greater importance than previously considered, and that the most likely valences are –2 for AsS, As_2 and S_2. Ioffe *et al.* (1985) investigated the Mössbauer spectra of pyrite, arsenopyrite and löllingite; their observations agree with the model of Tossell *et al.* (1981), as they found Fe to be divalent in all three minerals.

Crystal chemistry of pentlandite

In general terms, the composition of pentlandite is best described by the formula $(Fe,Co,Ni)_{9+x}S_8$, where *x* lies in the range –0.6 to 0.6 (Kaneda *et al.* 1986), although in standard references it is given as $(Fe,Ni)_9S_8$. The solid solution between Fe_9S_8 and Ni_9S_8 is limited to the central portions of the (pseudo-) binary. There is a complete solid-solution between $(Fe,Ni)_9S_8$ and Co_9S_8 in both natural (Petruk *et al.* 1969, Huhma & Huhma 1970) and synthetic pentlandite (Knop & Ibrahim 1961, Kojonen 1976, Kaneda *et al.* 1986). The metal:sulfur ratio in pentlandite has been reported to increase with Fe:Ni ratio and, partially, with temperature (Nickel 1970, Kaneda *et al.* 1986) as well as decreasing sulfur fugacity (Sugaki & Kitakaze 1998).

The crystal structure of synthetic Co_9S_8 was solved by Lindquist *et al.* (1936), and the same structure was determined for $(Fe,Ni)_9S_8$ (Pearson & Buerger 1956). This structure was later confirmed and refined (Knop & Ibrahim 1961, Hall & Stewart 1973, Rajamani & Prewitt 1973). The unit cell of pentlandite contains 32 metal atoms in tetrahedral coordination to sulfur and four metal atoms in octahedral coordination. The metal-bearing tetrahedra share three edges with adjacent metal-bearing tetrahedra, across which metal–metal bonds extend, thereby forming "cube clusters", each containing eight metal atoms. The cube cluster of eight atoms is in theory stabilized by 56 *d* electrons, requiring a 1:1 ratio between Fe and Ni, but allowing any amount of Co (Rajamani & Prewitt 1973). The octahedral site is more flexible and can contain any of Fe, Co, Ni, Ru, Ir, Pd or Ag (Hall & Stewart 1973, Makovicky *et al.* 1985, Cabri *et al.* 1996). The octahedral site prefers Ni to Fe at high temperatures and low pressures (Tsukimura *et al.* 1992), but this general relation may be modified by variations in the activities of Ni and Fe.

Analytical methods

The electron-microprobe analyses were performed on a Tracor Northern automated JEOL JCXA–733 Superprobe (wavelength dispersion). The accelerating voltage was set to 20 kV, and the beam current was 30 nA. The ZAF corrections were performed using an online program supplied by JEOL. The arsenic-containing phases were initially analyzed using Fe*K*α, Co*K*α, Ni*K*α, S*K*α, As*L*α, Sb*L*α, Bi*L*α and Au*L*α, although this was subsequently reduced to Fe, Co, Ni, As and S as the other elements were found to be below the detection limit. The sulfides were analyzed using S*K*α, Fe*K*α, Co*K*α, Ni*K*α, Cu*K*α, Zn*K*α, As*L*α, Ag*L*α, Sb*L*α, Au*L*α and Bi*L*α. The number of elements was later reduced to Fe, Co, Ni, Cu, Zn and S in analyses of pyrrhotite, pentlandite, chalcopyrite, cubanite and sphalerite, because the concentrations of As, Ag, Sb, Au and Bi in these minerals were found to be below the limits of detection.

Chalcopyrite, sphalerite, bismuthinite and pure metals and elements were used as primary standards. The ASP 200 sample of Kretschmar & Scott (1976) was used as a secondary standard to correct the analytical data for all sulfarsenides, as well as löllingite. Synthetic troilite was used to correct the analytical data for pyrrhotite and smythite.

Small false concentrations of elements known not to be present in the standards were detected in both the primary and the secondary standards. These concentrations define the detection limit of the elements considered. Element concentrations lying in the ranges shown in Table 2 were treated as absent in the phases investigated unless other observations indicated their presence. The values in Table 2 are based on 47 analyses of ASP 200 and 42 of synthetic troilite.

Mineralogy and textures of the investigated ores

The mineralogical differences among the three occurrences of mineralization at Arroyo de la Cueva are shown in Table 3, which lists minerals according to textural type, mineral association and location. The heading *Type* refers to the textural descriptions presented in the following paragraphs. These are labeled I to VI according to their relative age. *Mineral Association*

TABLE 2. FALSE CONCENTRATIONS IN SECONDARY STANDARDS

Standard	Co	Ni	Cu	Zn	As	Bi	Au	Sb
Troilite	0.08	0.04	0.06	0.12	0.10	0.19	0.10	0.19
Max.	0.18	0.16	0.17	0.49	0.30	0.75	0.47	0.70
Min.	0.01	0.01	0.01	0.01	0.01	0.01	0.01	0.01
σ	0.036	0.040	0.049	0.124	0.093	0.224	0.121	0.159
ASP 200	0.08	0.05	–	–	present	0.09	0.01	0.20
Max.	0.22	0.23	–	–	in	0.88	0.69	0.61
Min.	0.01	0.01	–	–	standard	0.00	0.12	0.01
σ	0.054	0.041	–	–		0.214	0.241	0.169

The above given concentrations define the detection limits of the given elements. They will vary according to analytical conditions and are not universally applicable. Concentrations are quoted in wt%.

TABLE 3. MINERAL ASSOCIATIONS IN THE ARROYO DE LA CUEVA DEPOSITS

	Mineral	Type	T from solvus (C°)	T from geotherm (°C)	Mina La Herrum-brosa	Mina Majar del Toro	Mina San Pedro
1A	Pyrrhotite	I	–	–	–	Scarce	–
	Pentlandite	I	330°-550°C	–	–	Common	–
1B	Pyrrhotite	I	–	–	Common	–	–
	Löllingite	I	–	–	Common	–	–
	Alloclasite	–	350°-550°C	–	Scarce	–	–
	Westerveldite	–	–	–	Very scarce	–	–
	Bismuth	–	–	–	Scarce	Scarce	–
2	Arsenopyrite	I + II	490°-630°C	540°-700°C	Scarce	–	–
	Cobaltite	(I) + II + III	280°-500°C	–	Scarce	–	–
3A	Löllingite	III	–	–	Scarce	–	–
	Arsenopyrite	IIIa	500-650°C *	420°-700°C	Scarce	–	–
	Magnetite	–	–	–	Common	Scarce	–
	Chlorite	–	–	–	Common	Scarce	Scarce
	Talc	–	–	–	Scarce	Scarce	Scarce
	Calcite	–	–	–	Scarce	Scarce	Scarce
3B	Arsenopyrite	IIIb + VI	>650°C *	280°-630°C	Common	Scarce	–
	Cobaltite	IV + V	<330°-450°C	–	Common	Common	–
	Löllingite	II	–	–	Scarce	–	–
	Maldonite	–	–	116°-373°C	Scarce	–	–
	Pentlandite	II	330°-550°C	–	–	Common	–
	Pyrrhotite	II	–	–	Abundant	Abundant	Scarce
	Chalcopyrite	–	–	–	Abundant	Abundant	Abundant
	Cubanite	–	–	–	Abundant	Abundant	Abundant
	Sphalerite	–	–	–	Scarce	Scarce	Common
	Gold	–	–	–	Scarce	Very scarce	Scarce
4	Arsenopyrite	V + VI	–	250°-285°C	Common	Scarce	–
	Pyrite	–	–	–	Scarce	Scarce	–
	Marcasite	–	–	–	Common	Abundant	–
	Smythite	–	–	–	Scarce	Scarce	–
	Violarite	–	–	–	–	Common	–
5	Chalcocite	–	–	–	–	Scarce	Common
	Covellite	–	–	–	–	Scarce	Common
	Goethite	–	–	–	Common	Common	Abundant
	Lepidocrocite	–	–	–	–	Scarce	Scarce

The minerals listed in the same group belong to the same association, and their relative age decreases as one moves down in the table. The first column indicate which *stage of mineralization* the association belongs to. The column entitled *Type* refers to the different textural and chemical groupings, which are described in the text. The column *T from solvus* refers either to minimum temperatures determined from the sulfarsenide solvus of Klemm (1965) or the pentlandite solvus of Kaneda *et al.* (1986). The column *T from geotherm* refers to temperatures determined using the arsenopyrite geothermometer (Kretschmar & Scott 1976) and from the stability of maldonite. (*) Indicates that a substantial part of the compositions lie within the exolution gap at 650°C. *Abundant*: equals 5 vol.% or more, *common*: 5–2 vol.%, *scarce* 1 vol.% or less, and *very scarce* means that only 1 or 2 grains of this phase were found. The abundance of phases was visually estimated.

refers to groups of phases that are found together. They are labeled 1 to 5 according to at which stage of mineralisation they formed, and A or B according to which phases physically occur together. *Stage 1* represents the primary ore-forming process, and *Stage 2*, the initial breakdown of the high-temperature phases. *Stage 3* represents the episode of hydrothermal alteration and metasomatism. *Stage 4* indicates the late hydrothermal alteration and possibly the earliest supergene alteration, whereas *Stage 5* is the late supergene weathering and desulfurization. These stages do not represent separate geological or metasomatic events, but the continuous evolution of the hydrothermal system.

The most distinct textural and mineralogical features of the Arroyo de la Cueva deposits are overgrowths and replacements, where several generations of a mineral overgrow earlier generations and phases. The compositions of the Fe–Co–Ni-bearing phases commonly reflect this, in that the Fe, Co and Ni contents vary according to the textural types, and most sulfarsenides are zoned. As and S contents are, in contrast, distributed in loosely defined groups with large overlaps between the differ-

ent textural types. The average compositions of the Fe–Co–Ni phases are listed in Table 4.

The veins cross-cutting the ore (Figs. 1G, H) are not described in detail, but they are proof of the omnipresence of hydrothermal alteration. The veins of chalcopyrite and cubanite, demonstrating ubiquitous lamellar intergrowths, are produced by exsolution from the intermedate solid-solution (*iss*) of the system Cu–Fe–S. This assumption is supported by abundant transformation-induced twins in chalcopyrite. The exolution of chalcopyrite and cubanite from *iss* must have occurred in the temperature interval 300–400°C, as the *iss* field shrank toward metal-poorer compositions (Craig & Scott 1982). This indicates initial temperatures above 300°C during the main metasomatism of the ore (*stage 3*).

Pyrrhotite

Pyrrhotite is the most common ore mineral in the Arroyo de la Cueva deposits. It occurs in association with all the other ore minerals, typically forming a matrix. The pyrrhotite matrix occurs as centimetric sized homogeneous masses, which commonly have been subject to alteration and deformation. The textures showing this are corrugation and disaggregation of lamellae, seen as subparallel lensoid discs or smaller equidimensional grains, which in turn form aggregates or mosaic textures. Parallel parting, probably along (0001), is very common and accentuated by weathering and replacement.

Electron-microprobe analyses show that the composition of the pyrrhotite varies widely, from almost 49.0

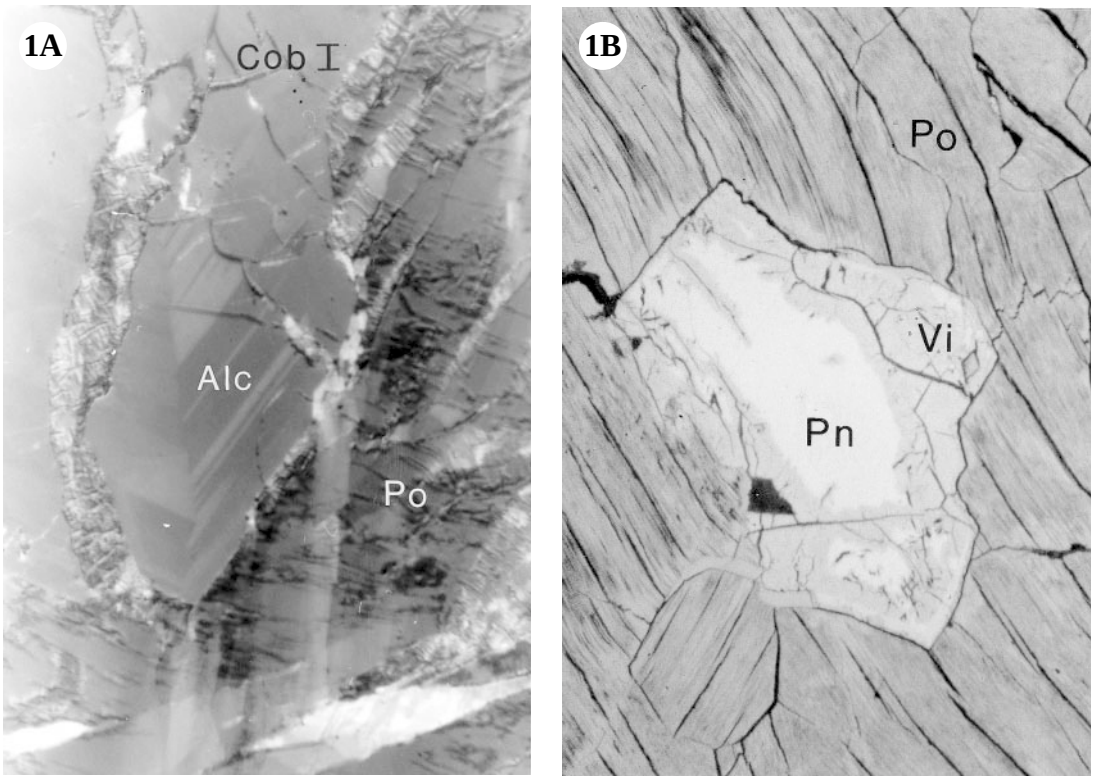

FIG. 1. Typical examples of textures produced by the alteration, metasomatism and deformation of the primary ore assemblage from Arroyo de la Cueva. Symbols: Alc alloclasite, Cb cubanite, Chl chlorite, Cob cobaltite, Cp chalcopyrite, Asp arsenopyrite, Mg Magnetite, Po pyrrhotite, Pn pentlandite, Vi violarite. A) Composite grain of alloclasite and cobaltite hosted in pyrrhotite. The alloclasite portions form clearly defined sectors, containing distinct sets of lamellae. There is no significant compositional variation from one lamella to another. The cobaltite domains of the grain show weak or no anisotropy, although different growth-induced layers can be discerned. B) A grain of pentlandite hosted in a mosaic of heavily deformed grains of Fe-poor pyrrhotite. Violarite replaces pentlandite from the margins and along cracks. C) Intergrown grains of löllingite (Lö I + II) and arsenopyrite (Asp I + II). Lö I is dusted with inclusions of native bismuth, as is Asp I. The latter forms pseudomorphs after Lö I, inheriting the bismuth inclusions. Lö II and Asp II overgrow Lö I and Asp I, forming a bismuth-free crust. The aggregate is enclosed in pyrrhotite. D) An aggregate of löllingite and arsenopyrite. The core of the aggregate consists of Lö I overgrown

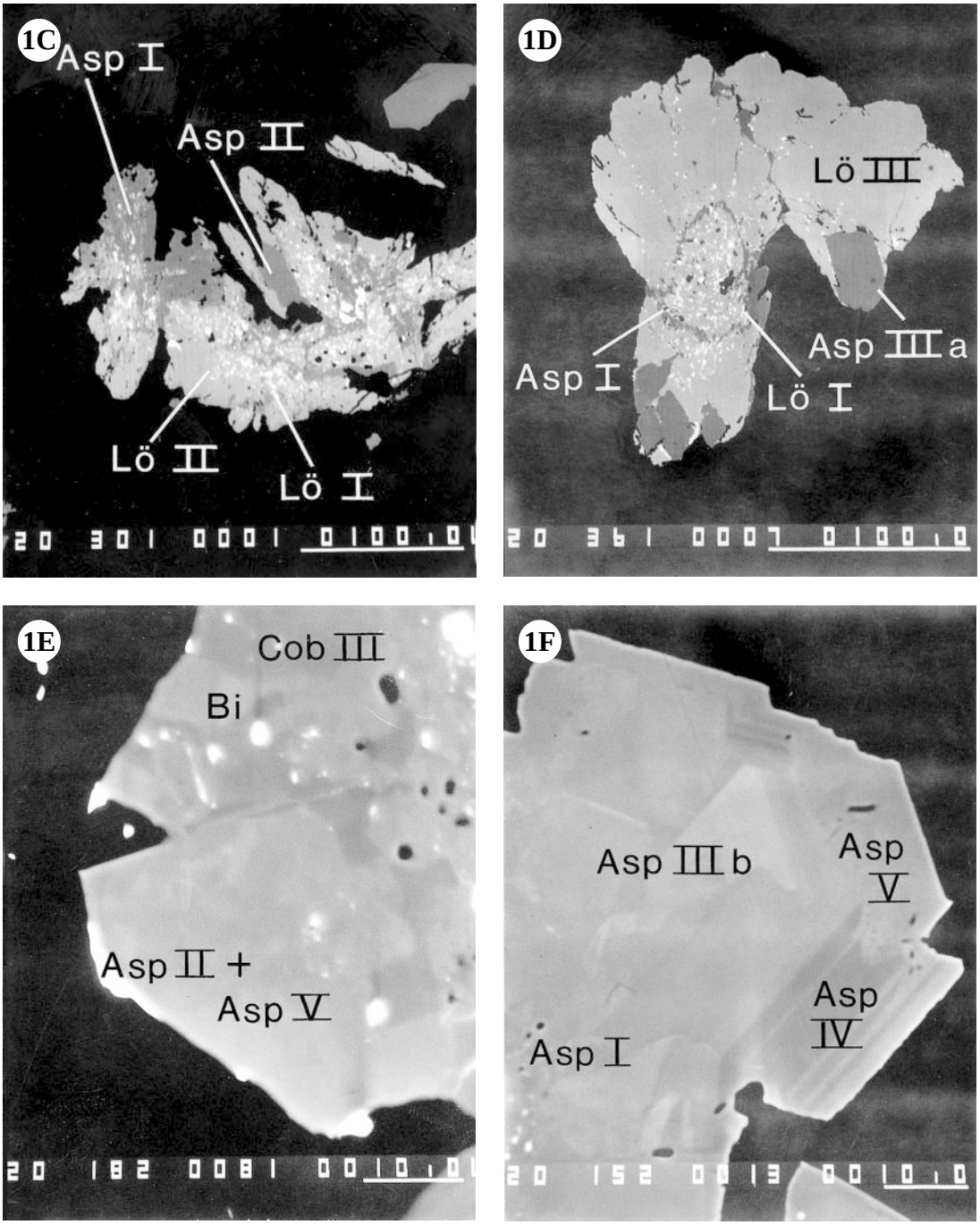

by a thin rim of Asp I. This core is overgrown and replaced by Lö III and Asp III. This process aligns the bismuth inclusions. The aggregate is hosted in a chlorite–magnetite vein. E) Arsenopyrite (Asp II + V) irregularly intergrown with cobaltite (Cob III) and native bismuth. The arsenopyrite shows diffuse internal zoning between Asp II (lighter grey) and Asp V (darker grey). F) An aggregate of arsenopyrite showing complex zoning and growth history. The sector-zoned mantle of the aggregate (Asp IIIb) overgrows the bismuth-dusted core (Asp I). The rim of the aggregate displays oscillatory growth-zonation (Asp IV), which in places has been eaten away by a more homogeneous phase (Asp V). This aggregate clearly illustrates the changing conditions (T–*X*) prevailing during the hydrothermal alteration of the ore.

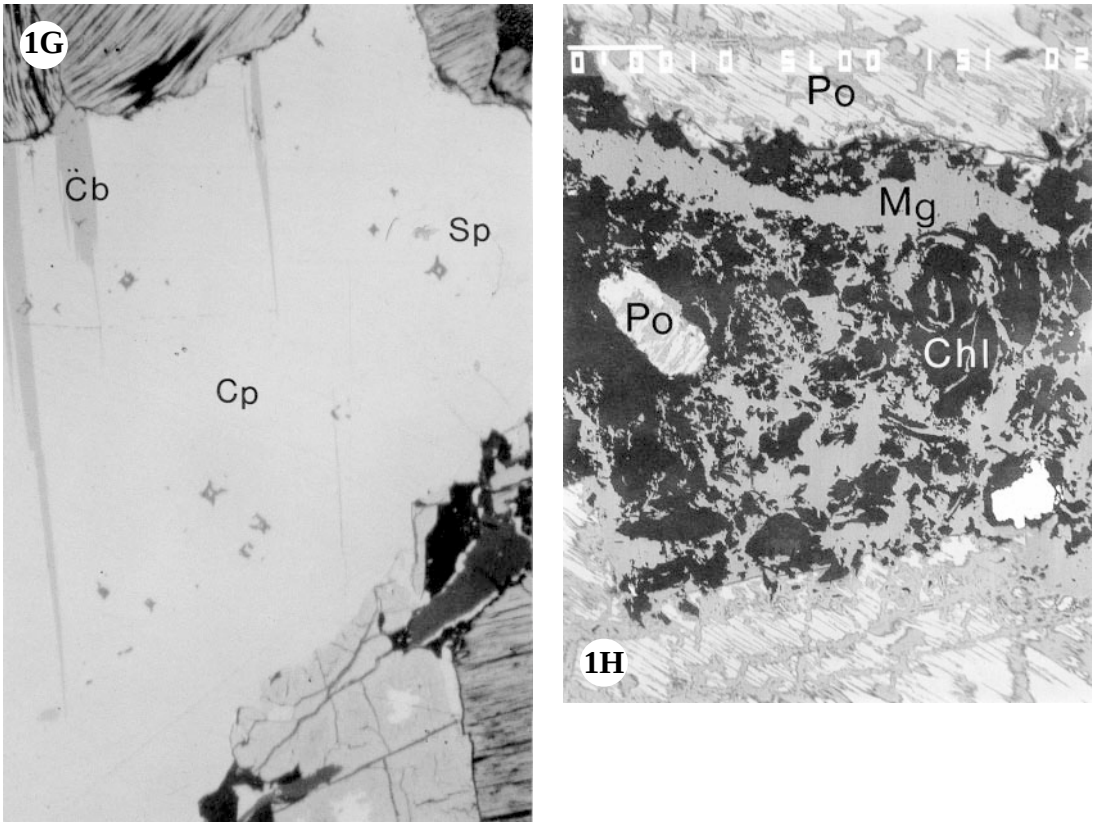

FIG. 1. (*continued*) G) Chalcopyrite–cubanite vein. In this case, the ratio of cubanite to chalcopyrite is relatively low. On average, it lies in the range 0.3 to 2. The star-shaped exsolution-induced bodies of sphalerite are well developed and contain a chalcopyrite core. The replacement of pentlandite by violarite seems to have occurred during the formation of the *iss* vein. H) Magnetite–chlorite vein that cross-cuts the pyrrhotite matrix, hosting minor arsenides and remnants of pyrrhotite. Pyrrhotite surrounding the vein is partially replaced by marcasite. Textures indicate that magnetite formed later than the chlorite, as it encloses and cross-cuts the latter. Figures 1A, B, G: 200×, oil immersion, A with crossed nicols. Figure 1H: 80×. All in reflected light. Figures 1C, D, E, F: BSE image. Scale bar shows size in micrometers.

to 45.0 at.% Fe. The contents of other metallic elements do not exceed the detection limits.

Where unaltered, the pyrrhotite is richer in Fe than is altered pyrrhotite. There is a substantial overlap between the two groups (Fig. 2). Compositional distributions similar to those shown by the Arroyo de la Cueva pyrrhotite have been shown to correlate with the magnetic and crystallographic properties of the pyrrhotite (Kontny *et al.* 2000, Pósfai *et al.* 2000). The compositions of unaltered pyrrhotite overlap the solid-solution fields of the intermediate-temperature forms, NC- and NA-pyrrhotite, and are richer in Fe than the solid-solution fields of the high-temperature MC and 1C forms (Scott & Kissin 1973). Two peaks in the compositional histogram, close to the compositions of 11C and 6C, indicate that these phases dominate in the unaltered pyrrhotite matrix. Pyrrhotite-11C and -6C most likely formed by transformation of pyrrhotite-NC or -NA as temperature decreased. Compositions richer in Fe than pyrrhotite-6C can be explained as intergrowths with submicroscopic troilite, whereas the compositions poorer in Fe are interpreted as intergrowths with pyrrhotite-5C or -4C. The altered pyrrhotite has a composition lying largely within the compositional field of the monoclinic pyrrhotite-4C, although there is an enigmatic peak around 45.6 at.% Fe and another close to 45.0 at.% Fe, which are attributed to the presence of smythite (Fe_9S_{11}).

Analyses made on tiny lath-shaped crystals of smythite growing in cracks in the pyrrhotite matrix gave the following composition (based on 11 analyses): 44.87 at.% Fe (σ = 0.21), 54.87 at.% S (σ = 0.25), and no concentration of any other element above 0.34 at.%. The average concentrations of these minor constituents (0.14 at.% Zn, 0.05 at.% Cu, 0.06 at.% Ni, 0.04 at.% Co) equal those found in the secondary troilite standard, indicating that they are analytical artefacts. The true Fe

TABLE 4. AVERAGE COMPOSITIONS OF THE Fe–Co–Ni PHASES

			Atomic Percent					Weight Percent					
		n	Fe	Co	Ni	As	S	Fe	Co	Ni	As	S	Total
Lo	I	22	23.41	5.34	4.89	62.21	4.15	19.44	4.67	4.27	69.25	1.99	100.28
	II	79	25.14	6.71	1.89	60.13	6.13	21.32	6.00	1.68	68.39	2.99	100.85
	III*	10	19.75	9.28	4.50	63.43	3.05	16.26	8.05	3.89	70.02	1.45	100.16
Asp	I*	25	27.82	2.61	2.61	38.07	28.90	27.34	2.70	2.70	50.17	16.30	99.45
	II*	15	27.53	3.88	2.27	37.94	28.39	27.01	2.35	4.00	49.89	16.00	99.73
	IIIa	7	22.19	6.73	3.97	37.66	29.45	21.77	4.10	6.93	49.50	16.61	99.25
	IIIb*	85	24.33	7.39	1.84	36.63	29.82	24.08	1.93	7.74	48.86	17.03	99.86
	IV	11	31.37	0.72	1.88	34.56	31.48	31.59	0.77	1.99	46.68	19.42	101.01
		8	29.46	1.35	3.05	34.72	31.41	30.13	1.46	3.28	47.63	18.44	100.94
	V	37	25.93	6.43	1.26	35.94	30.39	25.97	1.33	6.75	48.18	17.44	99.34
	VI	14	33.44	0.63	0.13	33.99	31.81	33.97	0.14	0.67	46.32	18.55	100.03
Pn	I*	16	17.86	21.89	12.59	N.A.	47.33	22.15	28.63	16.42	N.A.	33.68	101.05
	II*	27	19.47	20.59	13.23	N.A.	46.67	23.93	26.70	17.10	N.A.	32.94	101.52
Alc*		74	1.51	27.18	5.2	34.09	32.04	1.51	28.8	5.47	45.9	18.46	100.25
Cob	I*	61	1.39	29.6	3.51	33.09	32.43	1.38	31.44	3.7	44.68	18.74	99.99
	II	45	2.19	29.27	3.07	32.72	32.76	2.2	31	3.23	44.05	18.87	99.34
	III	16	1.19	30.45	2.35	34.01	32	1.2	32.51	2.48	46.12	18.58	101.08
	IV*	121	1.44	28.16	4.25	34.1	32.05	1.45	29.93	4.48	46.06	18.53	100.72
	V*	38	1.47	29.13	3.38	33.58	32.44	1.48	31.01	3.59	45.45	18.79	100.37

Concentrations below the estimated detection-limit (Table 1) were omitted before normalization to 100 at %. Symbols: Lö löllingite, Alc alloclasite, Pn pentlandite, Cob cobaltite, Asp arsenopyrite. N.A. indicates that the element in question was not sought. Those marked with * show large compositional variations.

content of this smythite can thus be calculated as 100 times [44.87 at.% Fe / (44.87 at.% + 54.87 at.% S)], giving 44.98 at.% Fe. Two compositions have been reported for smythite; the smythite from Arroyo de la Cueva almost perfectly fits Fe_9S_{11}, as found by Taylor & Williams (1972), and not the stoichiometry $Fe_{13}S_{16}$, as reported by Fleet (1982).

Pentlandite

Pentlandite is found within the pyrrhotite matrix. Its textural appearance is dependent on the degree of alteration and deformation of the matrix. Flame- or bleb-like bodies of pentlandite (Pn I) occur in unaltered pyrrhotite and are 10–100 μm in diameter, homogeneous and unaltered. Granular pentlandite (Pn II) is found in disaggregated and altered pyrrhotite and occurs as euhedral grains (40–150 μm) located at the junctions between the pyrrhotite grains (Fig. 1A). Mimetic replacement by violarite occurs along grain boundaries. Pn II seems to have formed by remobilization of Pn I during the disaggregation and alteration of the pyrrhotite matrix.

The compositional variation of pentlandite (Fig. 3) defines a line going from approximately $(Fe_{3.5}Co_{3.0}Ni_{2.5})_{\Sigma 9.0}S_8$ to $(Fe_{2.80}Co_{4.6}Ni_{1.80})_{\Sigma 9.2}S_8$. The Metal/S ratio does not vary along this line, but plots in distinct groups according to textural position, Pn I being richer in metal than Pn II. The latter type of pentlandite displays a positive correlation of Co *versus* (*Me*/S) and a negative correlation of Fe–Ni *versus* (*Me*/S).

Alloclasite

In the Arroyo de la Cueva deposits, alloclasite is found as large (500–2000 μm in diameter) sub- to euhedral grains within the pyrrhotite matrix. These grains contain well-defined sectors. In turn, these sectors contain lamellae that are parallel to the faces of the crystal. The thickness and number of lamellae vary from one sector to another. The very strong anisotropy of these zoned regions, along with the typical anisotropy in colors, confirm that the grains are alloclasite. The sector zoning closely resembles the hourglass textures commonly shown by arsenopyrite.

Alloclasite is invariably partially replaced by cobaltite, and thus loses its characteristic strong anisotropy and sector zoning (Fig. 1B). This replacement is pseudomorphic, and hence does not change the euhedral shape of the grains. This results in large composite grains of alloclasite and cobaltite. Such replacement of alloclasite by cobaltite has been attributed to the alloclasite–cobaltite transformation (Kerestejian 1984, Laroussi *et al.* 1992). The alloclasite–cobaltite transformation can be triggered by decreasing temperature or by increasing sulfur fugacity (Maurel & Picot 1974), and both factors seem to have been important in the Arroyo de la Cueva ores.

The variation in Fe, Co and Ni contents in alloclasite describes a continuous trend (Fig. 4). Almost all compositions of alloclasite follow this linear trend, regardless of growth lamellae and sector zones. The Co content

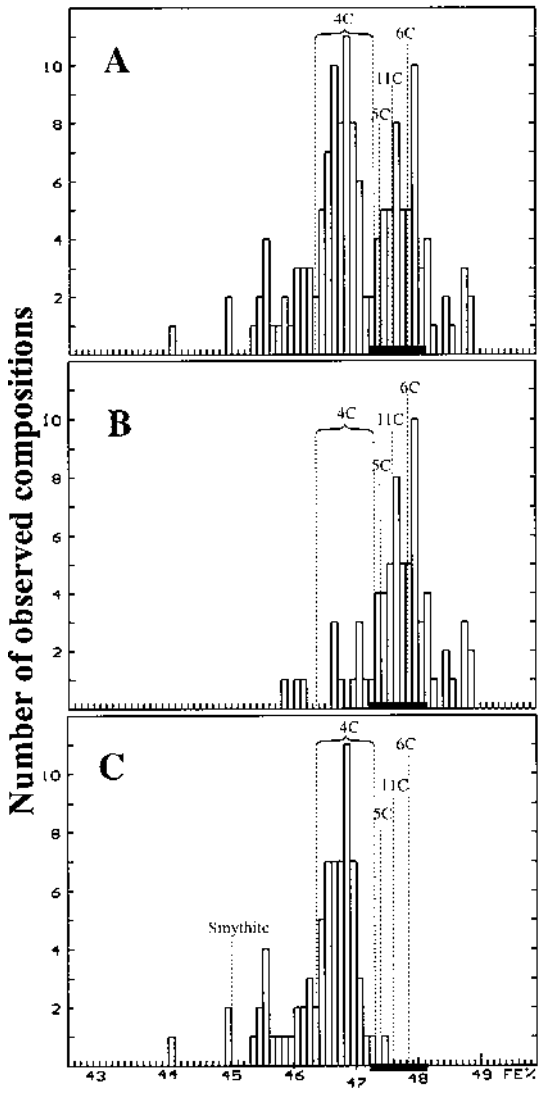

FIG. 2. Histogram of the iron content (at.%) in pyrrhotite from Arroyo de la Cueva. The compositions of the low-temperature pyrrhotite-4C, -5C, -11C and -6C, as well as that of smythite, are shown with dotted lines. The solid-solution field of pyrrhotite-NC is marked on the X axis with a black bar. A) All analyzed grains of pyrrhotite, regardless of textural position. B) Pyrrhotite from relatively unaltered aggregates (Type 1). Two peaks close to the compositions of 11C and 6C indicate these as dominant phases. C) Aggregates of altered pyrrhotite consist of monoclinic (4C) pyrrhotite with some grains significantly poorer in Fe (smythite).

varies from one lamella to another by up to 1 at.%, but the As–S content remains relatively constant within the grain. The bulk of the compositions describes a weak negative correlation between As and Co contents.

Löllingite

Löllingite occurs as an intergrowth of small (10–50 μm) anhedral grains, commonly forming aggregates with arsenopyrite or cobaltite. These aggregates are located either in the pyrrhotite or in chlorite–magnetite veins. Inclusions of bismuth are commonly found inside löllingite. Some grains are dusted with these inclusions, whereas they form parallel strings in others. A single grain of westerveldite (FeAs) was found intergrown with Bi-dusted löllingite. The löllingite was found to contain significant amounts of Co (3–10 at.%), Ni (1–7 at.%) and S (2–8 at.%) in addition to Fe and As. The areas dusted with Bi inclusions were scanned; the average Bi contents of the löllingite–bismuth aggregate were found to be 1.8–3.3 at.% Bi. On the basis of textures and mineral associations, it was possible to discern three compositionally distinct types of löllingite, Lö I to Lö III (Fig. 5). Lö I grains are dusted with bismuth inclusions and form aggregates. These aggregates are normally enclosed by the pyrrhotite matrix. Typical grains of Lö I are resorbed, and they are partially replaced by arsenopyrite and Lö II (Fig. 1C). The grains of Lö II are homogeneous and do not contain inclusions of bismuth. They mostly occur in aggregates with Lö I, which are replaced and overgrown by arsenopyrite and cobaltite. The third type of löllingite (Lö III) is mainly found inside the chalcopyrite–cubanite or chlorite–magnetite veins, and is not in direct contact with pyrrhotite. Lö III occurs as well-defined grains occasionally overgrowing or replacing Lö I (Fig. 1D). They can contain subparallel strings of inclusions of native Bi.

The textures described above indicate that löllingite grew during the primary episode of ore formation, and in the early stages of the hydrothermal alteration; first, Bi-bearing löllingite (Lö I) formed together with pyrrhotite and possibly westerveldite. The assemblage was then replaced and overgrown by "inclusion-free" löllingite (Lö II) and arsenopyrite. The composition of second-stage löllingite is poorer in Fe and S (Lö III) in areas where no pyrrhotite is present. This pattern indicates that reactions between the hydrothermal fluid and pyrrhotite locally buffered the activities of Fe and S.

Cobaltite

Cobaltite from the Arroyo de la Cueva deposits replaces and overgrows the earlier phases. It is found in five textural varieties, which have distinct but overlapping compositions (Fig. 4). Only Co, Fe, Ni, As and S were found in amounts higher than their detection limit. Cob I and Cob IV + V have compositions that describe linear trends in the Fe–Co–Ni triangle, whereas the compositions of Cob II and Cob III define loose groups.

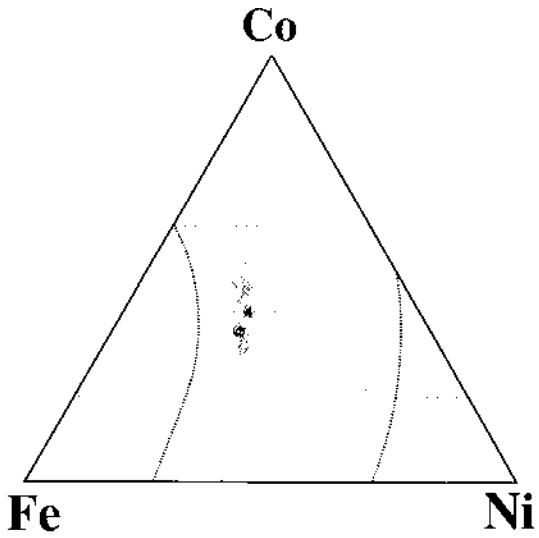

FIG. 3. Variation in the Fe, Co, and Ni contents and metal:sulfur ratio in pentlandite. The *Me*/S *versus Me* values (right-hand column) plot in two groups depending on textural position. The curved lines are the limits of solid solution outlined by Knop & Ibrahim (1961). Circles denote PnI, crosses, PnII.

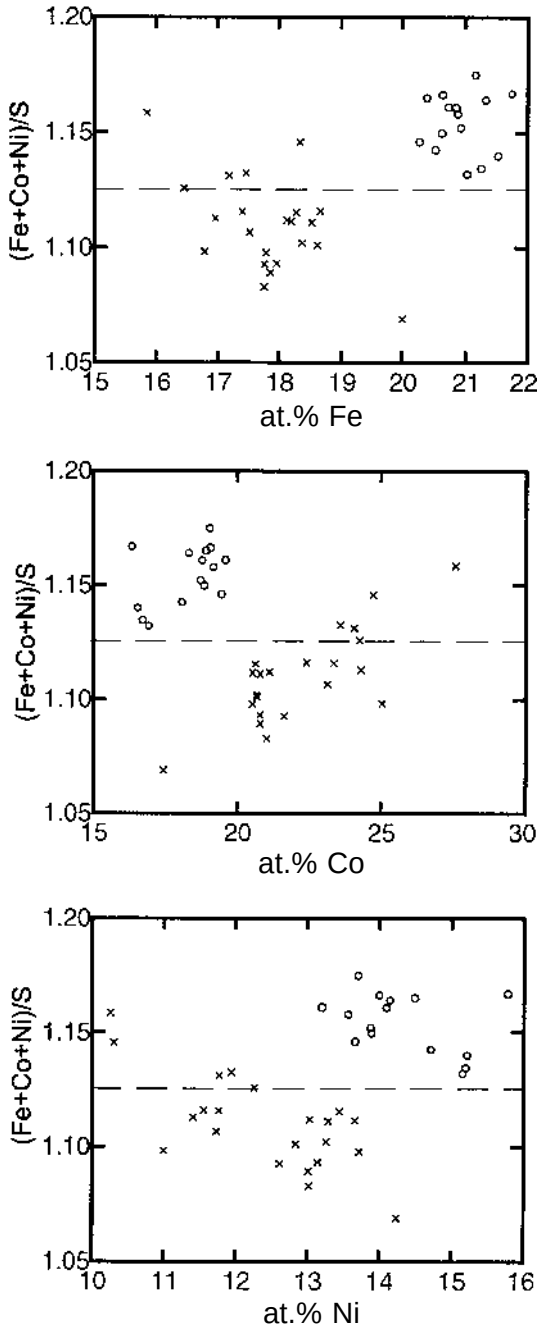

Pseudomorphic cobaltite found in alloclasite–cobaltite composite grains (Cob I, Fig. 1B), shows a compositional trend much like that of alloclasite. This could be inherited from the parent alloclasite. The compositional trend is slightly richer in Fe than that of alloclasite (Table 5).

The second and third type of cobaltite are found inside the pyrrhotite matrix, together with löllingite and arsenopyrite (Fig. 1D). Grains of Cob II forms irregular intergrowths together with arsenopyrite replacing Lö II. The grain size varies from small (Cob II ; 5–15 μm) Fe- and Ni-rich grains in the center to larger (Cob III; 10–50 μm) euhedral grains at the edges of the aggregates, which contain substantially more Co. Grains of Cob III were not found in direct contact with löllingite.

The most abundant type of cobaltite is found as well-defined euhedral grains (Cob V), which are 100–200 μm in diameter. These grains may display growth-induced zonation (Cob IV). These types of cobaltite are associated with the chalcopyrite–cubanite veins and are most likely contemporaneous. These types of cobaltite also replace pyrrhotite and overgrow composite grains of alloclasite and cobaltite. Cob IV and V evidently grew during the hydrothermal alteration the ore, and they display similar compositional trends. The cobaltite compositions are (Fe,Ni)-rich in the early stages, gradually evolving toward more stoichiometric compositions.

Arsenopyrite

Arsenopyrite commonly replaces and overgrows the other phases present in these ore deposits. Two main textural categories of arsenopyrite can be discerned:

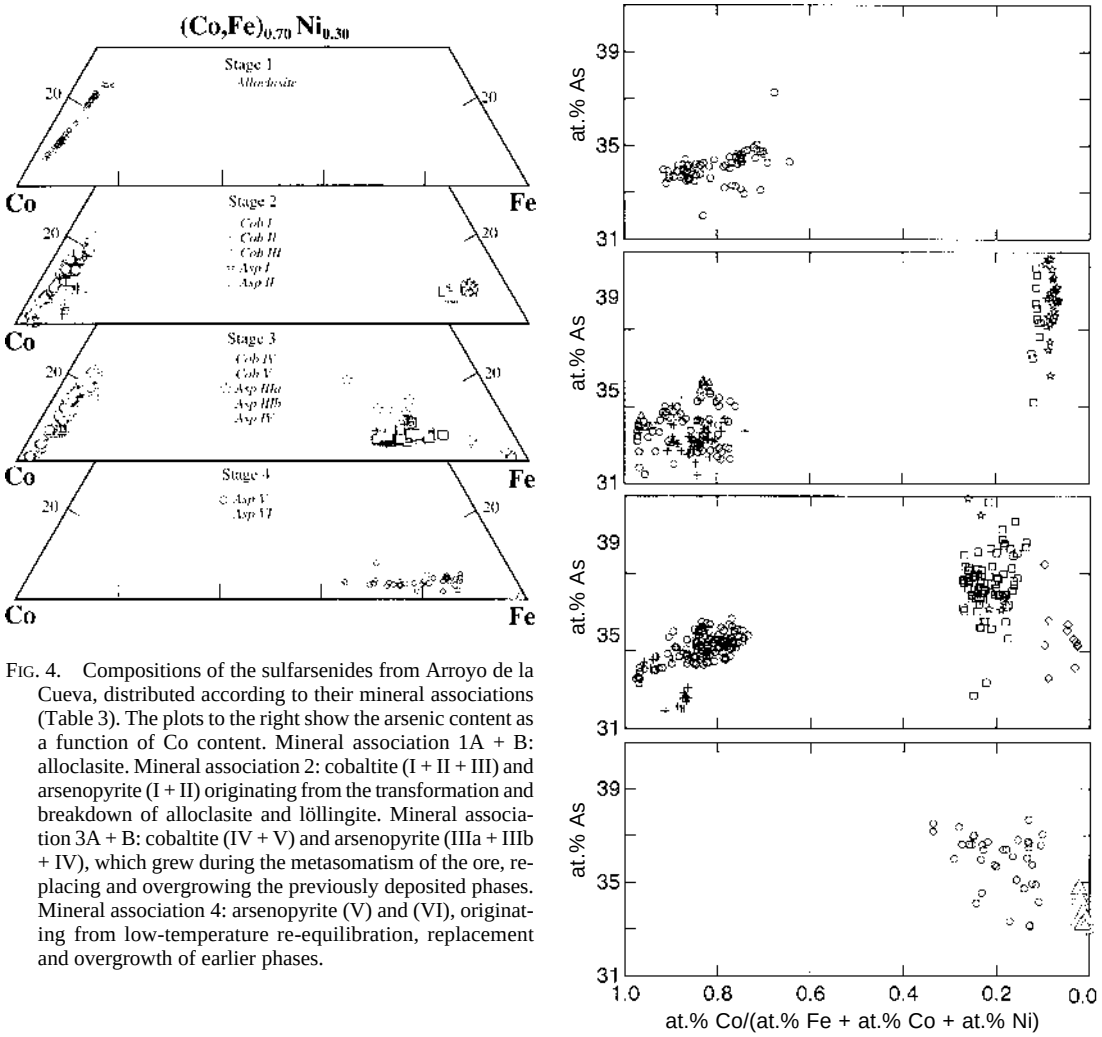

FIG. 4. Compositions of the sulfarsenides from Arroyo de la Cueva, distributed according to their mineral associations (Table 3). The plots to the right show the arsenic content as a function of Co content. Mineral association 1A + B: alloclasite. Mineral association 2: cobaltite (I + II + III) and arsenopyrite (I + II) originating from the transformation and breakdown of alloclasite and löllingite. Mineral association 3A + B: cobaltite (IV + V) and arsenopyrite (IIIa + IIIb + IV), which grew during the metasomatism of the ore, replacing and overgrowing the previously deposited phases. Mineral association 4: arsenopyrite (V) and (VI), originating from low-temperature re-equilibration, replacement and overgrowth of earlier phases.

small irregular grains associated with löllingite, cobaltite, pyrrhotite, bismuth, maldonite and gold, and massive impregnations and skeletal grains replacing pyrrhotite and overgrowing magnetite and chlorite. The small irregular grains of arsenopyrite are very heterogeneous on a micrometric scale. This large compositional variation is parallelled by variability in textures, and they are best described in terms of six compositional and textural types (Asp I, II, IIIa, IIIb, IV and V). The massive impregnations and skeletal grains are, on the contrary, more homogeneous (Asp VI). These compositional variations are shown in Figure 4.

Asp I occurs typically as poorly defined, resorbed grains 20–60 μm in diameter (Fig. 1C). They commonly enclose remnants of löllingite and are dusted with inclusions of Bi. Asp II consists of grains 40–100 μm in diameter, which may occur with Cob II (Fig. 1E). They replace and overgrow the intergrowths of Asp I, Lö I and Lö II. The growth of these grains has remobilized bismuth into larger grains and veinlets. Asp IIIa represents euhedral crystals of arsenopyrite intergrown with Lö III enclosed in the chlorite–magnetite veins (Fig. 1D). The crystals are 5–30 μm in diameter and diamond-shaped. Asp IIIb is the most common type of arsenopyrite. It is found as euhedral overgrowths on Asp I + II as well as on Lö I + II, but it also replaces pyrrhotite. Asp IIIb may contain tiny inclusions of maldonite. The Asp IIIb grains are 40–200 μm in size, and they usually contain triangular domains of different compositions (Fig. 1F). These domains form star- or hourglass-like textures, and are believed to be associated with the hourglass texture commonly seen in arsenopyrite. The composition varies between the different domains in the hourglass texture, which is seen as partitioning of (Co, Ni, As) *versus* (Fe, S). Asp IV overgrows Asp I–IIIb as

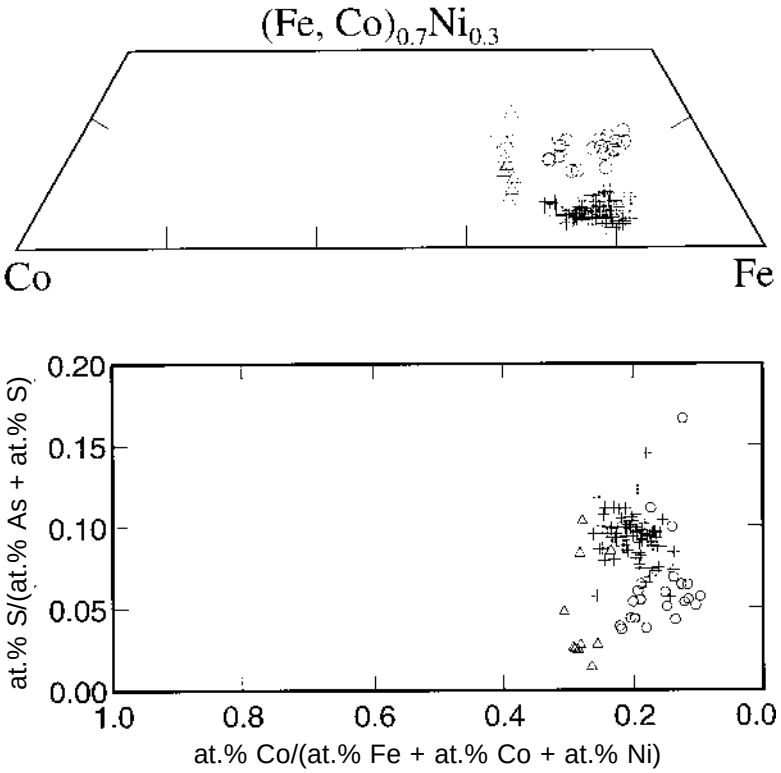

FIG. 5. The compositional variation exhibited by the various generations of löllingite. Lö I (circles) is found together with pyrrhotite + alloclasite ± westerveldite, and contains abundant inclusions of bismuth. Lö II (crosses) replaces Lö I, and does not contain inclusions. Lö III (triangles) was deposited in the chalcopyrite–cubanite veins and the magnetite–chlorite veins, not in contact with pyrrhotite.

well as pyrrhotite. This type of overgrowth consists of an oscillatory zonation, seen as layers 3–5 μm thick (Fig. 1F). Because these layers alternate between Fe-rich and Fe-poor compositions, they are shown as two compositions in Table 4. The group Asp V consists of partially re-equilibrated Asp I–IV (Fig. 1E). Certain zones in Asp I–IV are richer in Fe and S than the rest of the grain. Morphologically, this is seen as a small irregular variation in element distribution independent of cleavage and crystal faces. These textures are most likely produced by post-depositional diffusion and equilibration, indicating that arsenopyrite is not as refractory as previously assumed (Kretschmar & Scott 1976, Sharp et al. 1985). The last type of arsenopyrite (Asp VI) overgrows and replaces all the earlier sulfarsenides, löllingite or pyrrhotite (Fig. 1F).

ORE GENESIS

Textural evidence shows that the primary association is monosulfide solid-solution (*mss*) + löllingite + alloclasite at the Mina la Herrumbrosa mineralization, whereas it is *mss* subsequently exsolving pentlandite in Mina Majar del Toro and Mina San Pedro. An important observation is the mutual exclusion of löllingite and pentlandite, which indicates that in the presence of arsenic, Co and Ni preferentially concentrated in löllingite rather than in *mss*, which otherwise would exsolve pentlandite. This finding is in agreement with the observations of Gervilla *et al.* (1996), who found that As inhibits the formation of pentlandite, because Ni is partitioned into Ni arsenides.

The high Fe content of unaltered pyrrhotite suggests that pyrrhotite and löllingite were deposited on the metal-rich side of the pyrrhotite–löllingite join in the system Fe–As–S. This is supported by the grain of westerveldite hosted in löllingite. The effect of Co, Ni and of the presence of alloclasite on the phase relations in the system Fe–As–S is uncertain. Alloclasite only forms in As-rich environments (Maurel & Picot 1974), suggesting that the initial assemblage was *mss* + löllingite + alloclasite + westerveldite. Replacement of

TABLE 5. SUMMARY OF COMPOSITIONAL TRENDS IN SULFARSENIDES

No.	Reference	Paragenetic environment	Regression recalculated to formulae	N	R
1	Vinogradova *et al.* (1994): Vein hosted in ultramafic rocks	Cob–Ger together with Skt–Saf in an Au-bearing mineralization	$Co_{0.92-0.91-x}Fe_{0.08-0.09x}Ni_xAsS$ $0.03 < x < 0.73$	12	1.00
2	Mposkos (1983): Pegmatite in gneiss	Cob occuring with Po–Cp–Pn–Sp in a pegmatite lens	$Co_{0.87-x}Fe_{0.13-0.14x}Ni_{0.86x}AsS$ $0.02 < x < 0.32$	22	0.93
3	Fukuoka & Hirowatari (1980): Various manganese deposits containing Mn-bearing cobaltite–gersdorffite.	3.1 Fukumaki deposit: Cob–Ger with Nc–Mi–Saf–Py	$Co_{0.99-0.99x}Fe_{0.01-0.01x}Ni_xAsS$ $0.09 < x < 0.99$	8	1.0
		3.2 Tsutsumi deposit: Ger with Nc–Po–Py	$Co_{0.97-x}Fe_{0.07x}Ni_{0.03+0.93x}AsS$ $0.50 < x < 0.95$	8	0.91
		3.3 Fukadani and -guchi deposit: Cob–Ger with Nc–Po–Pn	$Co_{0.87-x}Fe_{0.13+0.07x}Ni_{0.93x}AsS$ $0.15 < x < 0.84$	8	0.97
4	Ixer *et al.* (1979): MSV-type ores in minor shales and carbonates	Tynebottom mine: Ger–Glc with Asp–Alc–Skt	$Co_{0.66-0.61x}Fe_{0.34-0.39x}Ni_xAsS$ $0.02 < x < 0.45$	6	1.0
5	Béziat *et al.* (1996). Spessartite-hosted	Cob–Ger with Po–Pn inclusions in Amp and Phl phenocrysts	$Co_{0.96-x}Fe_{0.04-0.30x}Ni_{0.70x}AsS$ $0.37 < x < 0.91$	14	0.99
6	Barkov *et al.* (1999): Hosted in a mafic intrusion	Cob–Ger containing PGE occurring with Po–Pn–Cp–Py	$Co_{0.93-x}Fe_{0.07-0.24x}Ni_{0.76x}AsS$ $0.14 < x < 0.57$	15	0.97
7	Gervilla *et al.* (1998): Interstitial to, or inclusions in, the silicates of an ultramafic intrusion	7a S/As ores: Cob–Ger with Nc–Po–Pn–Cp	$Co_{0.84-x}Fe_{0.16+0.05x}Ni_{0.95x}AsS$ $0.30 < x < 0.56$	70	0.91
		7b As ores: Cob found together with Nc–Mc	$Co_{0.96-x}Fe_{0.04+0.18x}Ni_{0.82x}AsS$ $0.08 < x < 0.39$	37	0.98
8	This study: Deposited by high-temperature magmatic fluids percolating the Ronda Peridotite. Occurring with Po, (Co,Ni)-rich Asp and Lö	8a Alloclasite formed with Fe-rich Po and Lö	$Co_{0.98-x}Fe_{0.17x}Ni_{0.02+0.83x}AsS$ $0.06 < x < 0.34$	74	0.99
		8b Cob I formed by mimetic replacement of alloclasite	$Co_{0.97-x}Fe_{0.03-0.03x}Ni_{0.97x}AsS$ $0.00 < x < 0.21$	61	0.99
		8c Cob IV + V. Replacing Po with Asp	$Co_{0.97-x}Fe_{0.03+0.07x}Ni_{0.93x}AsS$ $0.00 < x < 0.23$	159	0.99

Symbols: Amp amphibole, Alc alloclasite, Asp arsenopyrite, Cp chalcopyrite, Cob cobaltite, Ger gersdorffite, Mc maucherite, Mi millerite, Nc nickeline, Phl phlogopite, Po pyrrhotite, Pn pentlandite, Py pyrite, Saf safflorite, Skt skutterudite, Sp sphalerite. N: number of samples. R: correlation coefficient. R is to some extent artificially high because the parameters sum to a constant value.

löllingite by arsenopyrite started as sulfur fugacity increased and possibly as temperature decreased. The formation of arsenopyrite (Asp I + II) in coexistence with cobaltite (Cob I? + II + III) represents the initial breakdown of pyrrhotite and löllingite, and is called *stage 2*. This breakdown may have been triggered purely by a decrease in temperature, as the phases involved show little sign of metasomatism or hydrothermal alteration. During the metasomatism, which is designated as *stage 3*, löllingite (Lö II + III) continued to precipitate until the depositing fluid moved into the arsenopyrite–pyrrhotite binary field of the Fe–As–S system. They were precipitated together with cobaltite (I? + IV + V), arsenopyrite (III to VII), *iss*, spalerite and native Au. The sulfur fugacity was probably buffered by the presence of Fe-rich hexagonal pyrrhotite. The low-temperature hydrothermal alteration (*stage 4*) was responsible for the formation of marcasite, pyrite, smythite and violarite, whereas chalcocite, covellite, goethite and lepidocrocite formed during the late supergene weathering and desulfurization.

Geothermometry (Kretschmar & Scott 1976) applied to arsenopyrite replacing löllingite suggests temperatures in the range 600°–650°C during the earliest stage *(stage 2*) of alteration. The FeAsS–CoAsS–NiAsS solvus of Klemm (1965) indicates minimum temperatures of formation of alloclasite in the range 350°–550°C and of transformation of alloclasite to cobaltite in the range 300°–500°C (Fig. 7 in Klemm 1965). These observations support a high temperature of deposition of the assemblage *mss* + löllingite + alloclasite + westerveldite. However, both methods of temperature estimation are associated with large degrees of uncertainty. Co- and Ni-containing arsenopyrite, such as

observed in our study, has been shown to produce erroneously high estimates of temperature (Sundblad *et al.* 1984).

Using the pentlandite solvus diagram (Kaneda *et al.* 1986), the Arroyo de la Cueva pentlandite formed in the temperature range 330°–550°C and at log $f(S_2)$ values from –15 to –11, and probably at the low-temperature and low-fugacity end of this range. These low sulfur fugacities indicate that pentlandite formed in equilibrium with Fe-rich "hexagonal" pyrrhotite and correspond well with the presence of minor troilite in the "hexagonal" pyrrhotite aggregates. It is likely that the formation of the euhedral grains of pentlandite was coupled with the metasomatism of the ore, as they exhibit Co-enrichment trends in much the same way as the sulfarsenides.

The initial temperature of deposition of the primary pyrrhotite and its associated phases is very uncertain. It was probably close to 400°–550°C, as indicated by the compositions of the alloclasite and pentlandite. The 540°–700°C range indicated by the earliest replacement by arsenopyrite is probably erroneously high, whereas the 280°–420°C suggested by the compositions of cobaltite are the most likely temperatures for the *stage-2* alteration. Arsenopyrite and cobaltite compositions suggest temperatures up to 500°C for the main stage of hydrothermal alteration (*stage 3*). This is contradicted by the maldonite inclusions found inside Asp IIIb, as maldonite is stable only in the temperature interval 116°–373°C (Okamoto & Massalski 1983). Maldonite probably formed by reaction between the bismuth inclusions and Au contained in the metasomatic fluid.

An argument for a hydrothermal origin for all the observed phases is the Co-enrichment trend exhibited by the various Fe–Co–Ni-bearing phases. Even alloclasite exhibits this type of trend. This fact suggests that the primary mineral association (*stage 1*) was formed during the same sequence of hydrothermal processes as those which subsequently metasomatized the ore.

Discussion of the Compositional Trends

Mineralogical evidence from Arroyo de la Cueva suggests that the compositional trends observed in the Fe–Co–Ni-bearing phases are linked to the hydrothermal alteration of the ore. The most distinct trends are shown by cobaltite and alloclasite, but pentlandite also displays such compositional variation. Arsenopyrite and löllingite show equally large variations in their contents of Fe, Co and Ni, but these variations are only vaguely linear, if at all.

The best way of describing these (Fe,Co,Ni)-trends is by producing statistical regressions. All regression lines discussed in the following paragraphs were calculated using molar proportion of Fe, Co and Ni divided by the sum of metals. The sum of Fe, Ni and Co being constant, any combination of the three elements could be chosen as dependent and predictive variables, yielding practically the same lines. This enables comparison of data from various minerals and sources.

The sulfarsenide trends that pertain to the Arroyo de la Cueva minerals (8a, 8b and 8c in Table 5) show that Ni and Fe substitute for Co in different proportions, depending on the paragenetic situation. All three trends begin close to the Co corner and end on the Fe–Ni join. The alloclasite trend, 8a, starts on the Co–Ni join (0.02 Ni). The two cobaltite trends, 8b and 8c, start on the Co–Fe join (0.03 Fe). The trends (8a, 8b, 8c) intercept the Fe–Ni join at 0.83, 0.88 and 0.90 Ni, respectively.

These trends were compared to similar trends in other deposits. Compositions from a number of sulfarsenide occurrences that display significant trends are shown in Figure 6. These sulfarsenides were deposited in various geological environments, although most of them are related to ultramafic to mafic magmatic activity. A summary of these deposits and their characteristics is given in Table 5, along with the results of this study. The data are presented as cation proportions [*Me*/(Fe + Co + Ni)] and anion proportions [*X*/(As + S)]. This approach neglects the observed variations in the metal:anion ratio, which most likely were produced by differences in the experimental conditions and in the selection of standards. Statistical outliers and compositions rich in elements other than Fe, Ni, Co, S and As have been omitted.

The equations of the regression lines are listed in Table 5, along with the basic statistical parameters. The regression lines are shown in Figure 7. From this figure and the corresponding equations, it is clear that the trends of substitution vary from occurrence to occurrence and from association to association. The trends can be divided into three groups: a) Ni/Fe trends (trend 2, 3c, 5, 6, 7a, 7b, 8a), where Co is replaced by a mixture of Fe and Ni, b) Ni trends (3a, 3b, 8b, 8c), where Co is replaced predominantly by Ni, and c) Co/Fe trends (1, 4), where Ni is replaced by a mixture of Co and Fe. When comparing these trends with the reported assemblages, the following relations emerge. The Ni/Fe trends correspond to occurrences where the sulfarsenides formed in the presence of monosulfides and monoarsenides, in addition to phases such as maucherite or pentlandite, indicating a metal-rich environment. The Ni trends are found in sulfarsenides, which formed in the presence of sulfarsenides, disulfides or diarsenides, as well as pyrrhotite or nickeline, suggesting that the anion fugacities were inside the *Me*As–*Me*AsS–*Me*$(As)_2$ or the *Me*S–*Me*AsS–*Me*$(S)_2$ field. The Co/Fe trends are

Fig. 6 (following pages). Compilation of sulfarsenide compositions from the literature, in terms of atomic proportions in the Co–Fe–Ni triangle and as orthogonal plots of As/(As + S) *versus* Co/(Fe + Co + Ni). Source references are summarized in Table 5.

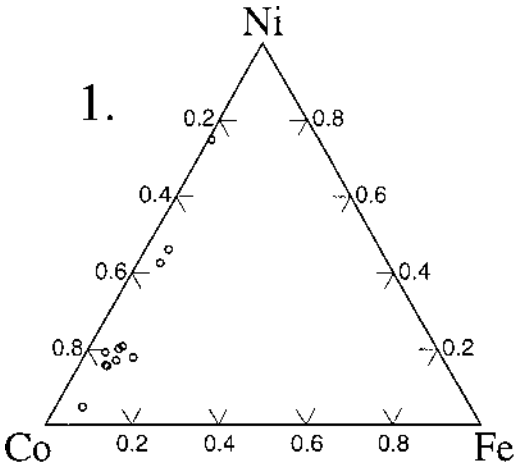
1.
Ni
Co
Fe
0.2
0.4
0.6
0.8

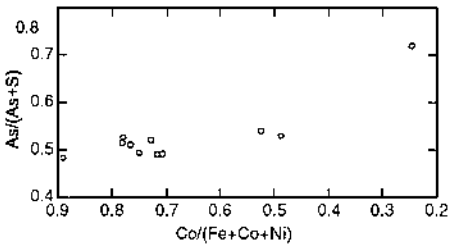
As/(As+S)
Co/(Fe+Co+Ni)

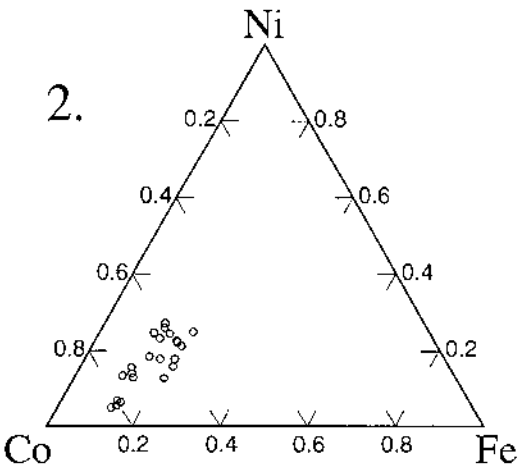
2.
Ni
Co
Fe
0.2
0.4
0.6
0.8

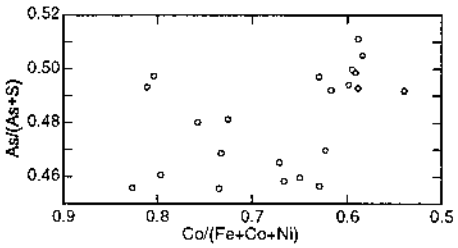
As/(As+S)
Co/(Fe+Co+Ni)

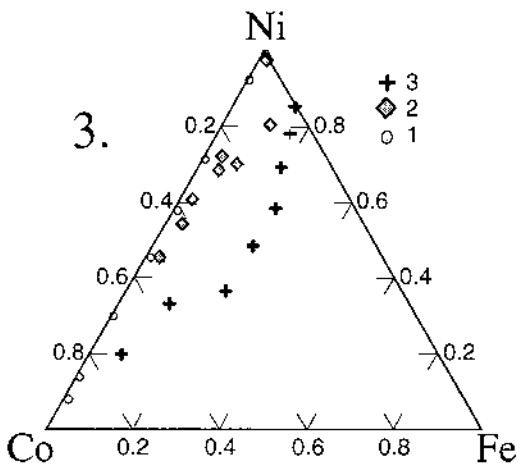
3.
Ni
Co
Fe
3
2
1
0.2
0.4
0.6
0.8

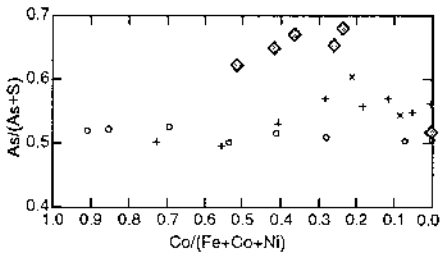
As/(As+S)
Co/(Fe+Co+Ni)

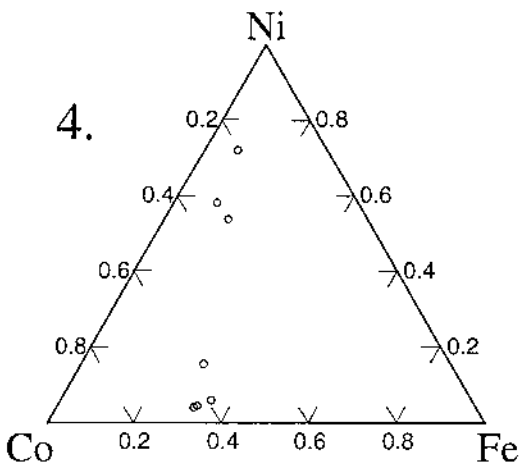
4.
Ni
Co
Fe
0.2
0.4
0.6
0.8

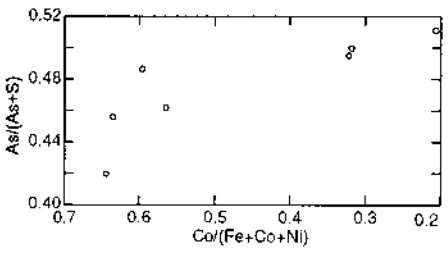
As/(As+S)
Co/(Fe+Co+Ni)

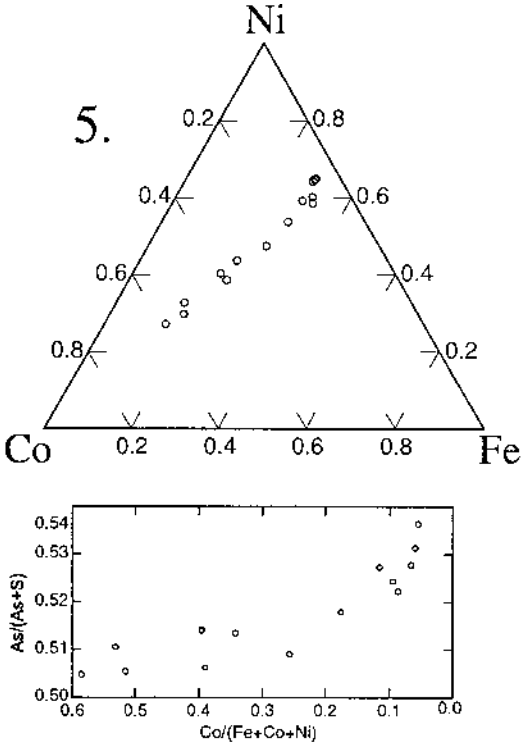
5.
Ni
Co
Fe
0.2
0.4
0.6
0.8
As/(As+S)
Co/(Fe+Co+Ni)

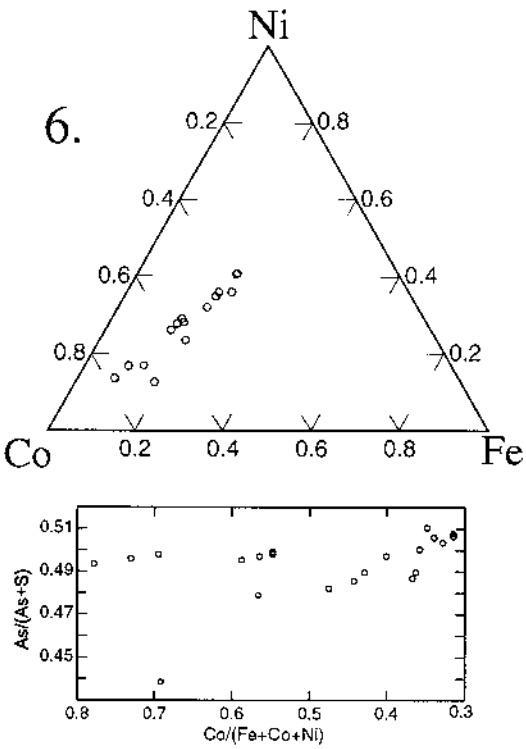
6.
Ni
Co
Fe
0.2
0.4
0.6
0.8
As/(As+S)
Co/(Fe+Co+Ni)

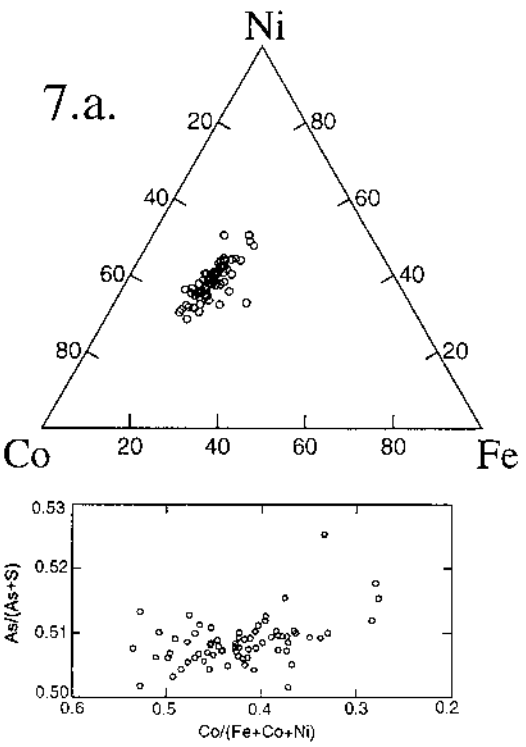
7.a.
Ni
Co
Fe
20
40
60
80
As/(As+S)
Co/(Fe+Co+Ni)

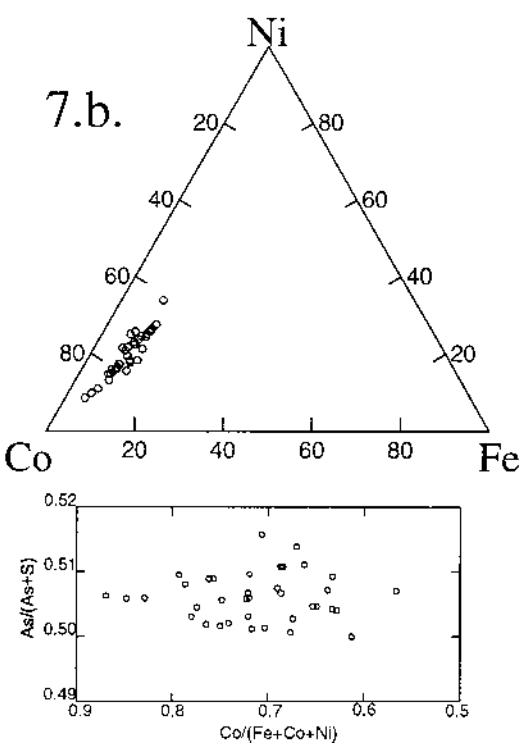
7.b.
Ni
Co
Fe
20
40
60
80
As/(As+S)
Co/(Fe+Co+Ni)

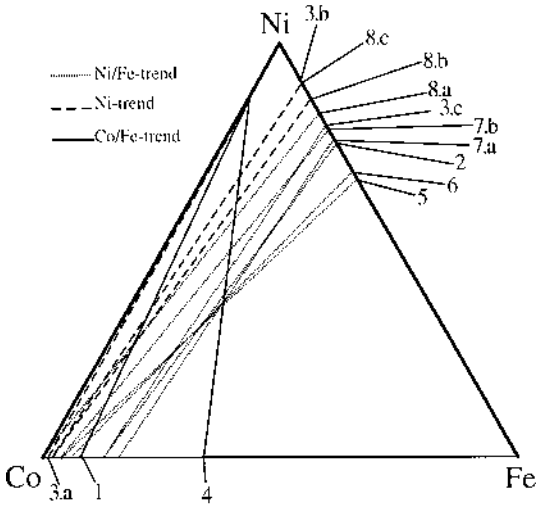

FIG. 7. Linear regressions derived from the datasets in Figure 6. Equations and statistical parameters are given in Table 5. Three types of trends can be distinguished. They are dependent on the mineral association in which the sulfarsenides occur.

found in associations containing skutterudite as well as sulfarsenides or diarsenides, suggesting an environment with high fugacity of arsenic. There is little correlation between the As/(As + S) and the Co/(Fe + Co + Ni) values (Fig. 6). In some cases (trends 1, 4 and 5), vague negative correlations can be recognized, and both Co/Fe trends are among these.

By applying the iso-electronic model (Hulliger 1968, Nickel 1968), it is possible to estimate valences of the cations and of the anion group. The cation valences were calculated by adding the *d* plus *s* electrons minus the 6 nonbonded *d* electrons in the pyrite- and marcasite-type sulfides. The corresponding anion valences are equal to $-2 + [-2\ As/(As + S)]$, assuming As_2^{4-}, AsS^{3-} and S_2^{2-} (Fig. 8). It should be noted that in this calculation, the absolute valences are arbitrary, but the relation between them is real. Most of the compositions quoted in Table 5 and used in Figures 6 and 7 have anion valences very close to –3, and cation valences from +2.9 to +3.1. There is a relatively large variation in the valence of the cations (average equal to +3.10, $\sigma = 0.09$), which is not matched by a similar variation in the anion valence (–3.02, $\sigma = 0.03$). The model-valences are compared to the line defined by the iso-electronic model (Fig. 8), clearly showing a difference between observed and predicted behavior for the bulk of the compositions. A dif-

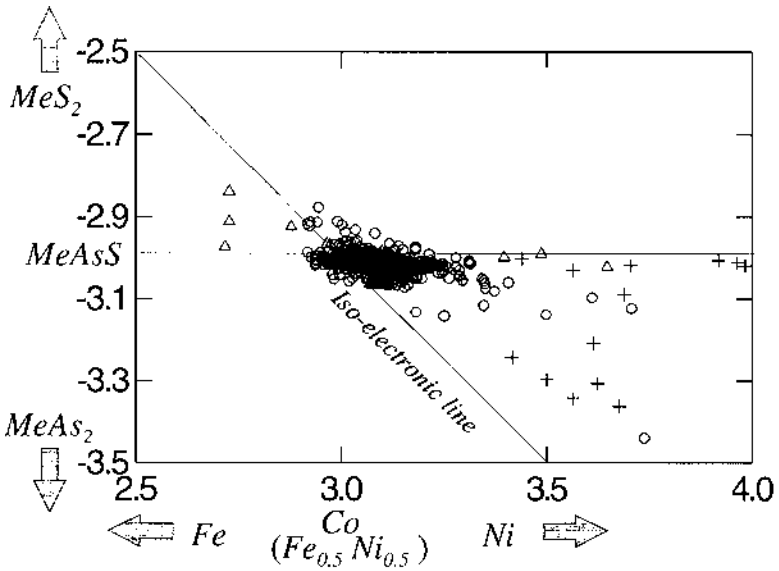

FIG. 8. Calculated valences for the data presented in Figure 6. The valences were calculated assuming that both the *d* and *s* electrons of the metal participate in bonding, and that six nonbonding *d* electrons are present in pyrite-type structures. + Ixer *et al.* (1979), Δ Fukuoka & Hirowatari (1980), ○ all remaining compositions.

ferent pattern is shown by the outlying cases, which define a weak correlation parallel to the iso-electronic line. This line lies on the sulfur-rich side of sulfur-rich compositions and on the arsenic-rich side of arsenic-rich compositions. Note also that no sulfur-rich compositions have cation valences above the average (+3.10), whereas no arsenic-rich compositions have cation valences below the average. It thus seems that the As-for-S substitution is restricted to the area between the model-valence line and the *Me*AsS line. The sulfur- and arsenic-rich compositions can thus be explained by cation valences lower and higher, respectively, than predicted by the iso-electronic model.

In the Arroyo de la Cueva material, distinct compositional patterns are followed by alloclasite and cobaltite on the one hand and arsenopyrite on the other (Fig. 9). Arsenopyrite shows large variations in the contents of Fe, Co and As, whereas alloclasite and cobaltite show large variations in the contents of Co and Ni and a much more restricted variation in the arsenic content. The Ni–As plot in particular reveals two distinct patterns of variation. The compositions of arsenopyrite show a broad positive correlation of 0.5 at.% Ni for 1 at.% As, whereas the cobaltite and alloclasite compositions show a correlation with a ratio of 4–8 at.% Ni for 1 at.% As. The correlations meet around 33 at.% As and

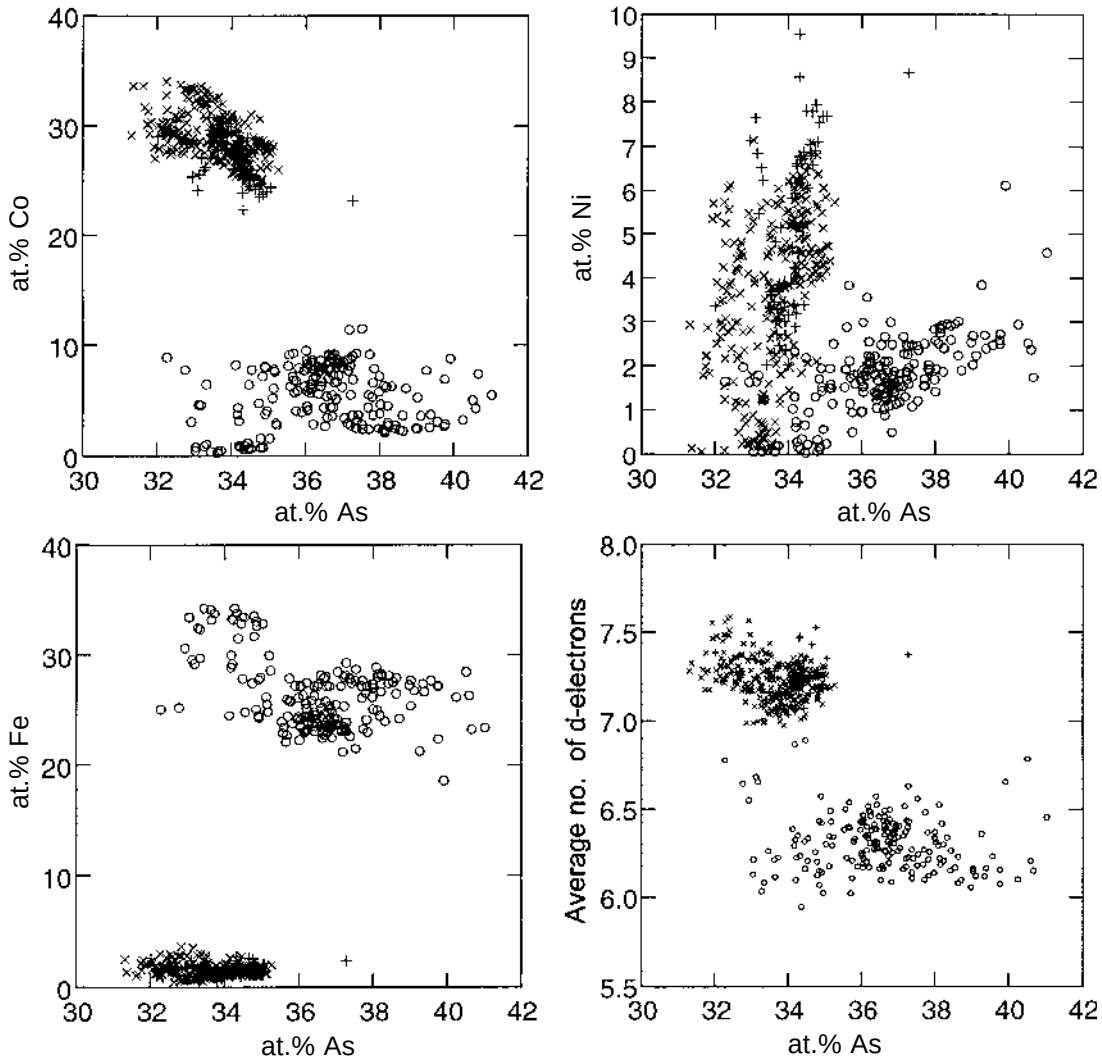

FIG. 9. Compositional variation in the sulfarsenides from Arroyo de la Cueva shown as at.% *Me versus* at.% As and number of *d* electrons *versus* at.% As. Distinct patterns are followed by arsenopyrite (○) compared to alloclasite (+) and cobaltite (×).

0 at.% Ni, and only a few compositions fall between the two main clusters, all of these belonging to the Asp IIIa category. A plot of the number of *d* electrons *versus* at.% As show two distinct clusters, an arsenopyrite cluster (6–6.5 *d* electrons, 33–41 at.% As) and an alloclasite–cobaltite cloud (7–7.5 *d* electrons and 32–35 at.% As); again, it is the Asp IIIa category that falls between the two groups. These observations point to two different schemes of substitution, one followed by alloclasite and cobaltite, and one followed by arsenopyrite. The alloclasite–cobaltite scheme shows little interdependence between the extent of As-for-S substitution and of substitutions involving Fe, Co and Ni. On the contrary, the arsenopyrite scheme shows a strong correlation between the substitutions. As already mentioned above, the Ni/As correlation in arsenopyrite has a negative influence on the reliability of the temperatures inferred using the arsenopyrite geothermometer.

The regression line describing the composition of pentlandite from Arroyo de la Cueva, [Fe/(Fe + Co + Ni) = 0.12 + 0.976 • Ni/(Fe + Co + Ni), $R = 0.818$], is of a similar nature to the Ni/Fe trends in the sulfarsenides, but involves compositions much richer in Fe. Starting with a surplus of iron, Co substitutes for Fe and Ni in a ratio close to 1:1. The trend cuts the Fe–Ni join at $Fe_{0.55}Ni_{0.45}$, and the Co–Fe join at $Co_{0.88}Fe_{0.12}$, maintaining the surplus of Fe over Ni, ΔFe = [(at.% Fe – at.% Ni)/ΣMe]. Only the central part of the trend ($Co_{0.33}$ to $Co_{0.51}$) is represented by measured compositions. The compositions of the Arroyo de la Cueva pentlandite are compared (Fig. 10) with pentlandite from the Bushveld Intrusion (Merkle & von Gruenewaldt 1986) and Outokumpu (Huhma & Huhma 1970). In all three cases, Co substitutes for Fe and Ni in a linear fashion. The data from Bushveld form an extension of those from Arroyo de la Cueva, following the same trend, whereas those from Outokumpu follow a parallel trend. These trends run perpendicular to the Fe–Ni join in the Fe–Ni–Co diagram, but diagonally in a Co *versus* Fe/Ni diagram. The latter type of relations can also be seen in the data compiled by Riley (1977). All these pentlandite compositions occur in mineral assemblages much like the one at Arroyo de la Cueva and in deposits associated with the alteration of ultramafic rocks. Hydrothermal remobilization generally enriches pentlandite in cobalt, and has not been considered to affect the Fe/(Fe + Ni) value (Merkle & von Gruenewaldt 1986). The pentlandite from Arroyo de la Cueva, Outokumpu and Bushveld shows trends that maintain the ΔFe value but not the Fe/(Fe + Ni) value.

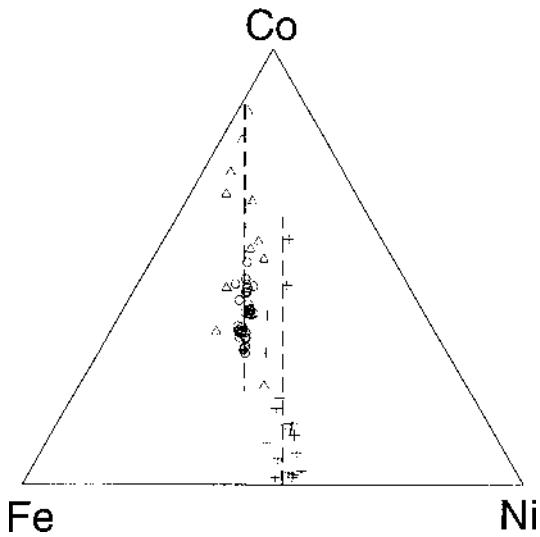

FIG. 10. Compositional trends for pentlandite from Outokumpu, Bushveld and Arroyo de la Cueva show trends in compositional variation. The Arroyo de la Cueva trend overlaps with the Bushveld trend, whereas the Outokumpu trend is richer in Ni, although parallel. ❍ This study, Δ Merkle & von Gruenewaldt (1986), + Huhma & Huhma (1970).

The trend ($Fe_{1+0.5x}Co_{8-x}Ni_{0.5x}$) exhibited by pentlandite from Arroyo de la Cueva and the Bushveld suite suggests that Fe occupies the octahedral site, whereas the tetrahedral sites are occupied by equal amounts of Fe and Ni. Co substitutes for Fe and Ni in the tetrahedral clusters in a 1:1 ratio, thus maintaining the electron count in the clusters. The compositional trend corresponds to the Fe-rich limit of the bonding model suggested by Hall & Stewart (1973) and Rajamani & Prewitt (1973). This model suggests that the number of non-bonding *d* electrons must be maintained at an average of 7 in the tetrahedral sites, and that the octahedral site is flexible (*i.e.*, ΔFe may equal –0.11 to 0.11). The pentlandite from the Outokumpu suite lies within the limits of this model, having a ΔFe of –0.04. This equals 0.32 Fe and 0.68 Ni on the octahedral site, assuming that all Co is tetrahedrally coordinated and the Fe:Ni ratio in tetrahedral sites is 1. Kaneda *et al.* (1986) showed that the Fe/Ni value in pentlandite is dependent on sulfur fugacity and temperature, a high fugacity of sulfur and low temperatures favoring high Ni contents. These variables had to be relatively constant during the (re-)crystallization to produce the above-mentioned trends. If the hydrothermal fluid remobilizing pentlandite was in equilibrium with hexagonal pyrrhotite, the activities of Fe and S would be buffered, producing exactly the observed effect.

CONCLUSIONS

The Arroyo de la Cueva occurrences formed as a result of hydrothermal alteration of a mineral association initially deposited at high to intermediate temperatures and low fugacity of sulfur. The formation of the ore occurrences can be divided into five main stages. *Stage 1*: Primary mineralization depositing *mss* ±

löllingite ± alloclasite ± westerveldite ± pentlandite. *Stage 2*: Initial replacement of pyrrhotite, löllingite and alloclasite by arsenopyrite and cobaltite. *Stage 3*: Main hydrothermal alteration mainly forming *iss*, arsenopyrite, cobaltite, maldonite and native Au, as well as remobilizing pyrrhotite and pentlandite. *Iss* breaks down to chalcopyrite, cubanite and sphalerite. *Stage 4*: Late-stage hydrothermal alteration where smythite, marcasite and pyrite replace pyrrhotite, and violarite replaces pentlandite. *Stage 5*: Supergene oxidation and desulfurization responsible for the formation of chalcocite, covellite, goethite, hydrated goethite and lepidocrocite.

The compositional trends observed in sulfarsenides were found to be dependent on the mineral association. Three groups of trends were distinguished: a) trends where Co is replaced by a mixture of Fe and Ni, b) trends where Co is replaced predominantly by Ni, and c) trends where Ni is replaced by a mixture of Co and Fe. These trends formed in environments of distinct fugacities of As and S, a) formed at relatively low fugacities, b) at intermediate fugacities, and c) at high fugacities.

The compositional trends of pentlandite lie on the Fe-rich limit (Arroyo de la Cueva, Bushveld), or within the limits (Outokumpu), of the compositional range of the bonding models suggested by Rajamani & Prewitt (1973) and Hall & Stewart (1973). In the Arroyo de la Cueva suite, the hydrothermal remobilization of pentlandite occurred in equilibrium with pyrrhotite, which explains why the trend lies at the Fe limit of the solid solution. Cobalt, on the other hand, was geochemically unbuffered and crystal-chemically unconstrained. It therefore shows a large variation in concentration, producing the observed trend.

Acknowledgements

The assistance of Mr. J. Fløng and Mrs. B. Wenzel is gratefully acknowledged. The electron-microprobe analyses were financed by the Danish Natural Research Council, and the field work, by the University of Copenhagen. Constructive comments of D. Béziat, R.A. Ixer and R.F. Martin improved this contribution significantly.

References

Barkov, A.Y., Thibault, Y., Laajoki, K.V.O., Melezhik, V.A. & Nilson, L.P. (1999): Zoning and substitutions in Co–Ni–(Fe)–PGE sulfarsenides from Mount General'skaya layered intrusion, Arctic Russia. *Can. Mineral.* **37**, 127-142.

Bayliss, P. (1968a): The crystal structure of disordered gersdorffite. *Am. Mineral.* **53**, 290-293.

_____ (1968b): The different crystal structures of gersdorffite (NiAsS). *Can. Mineral.* **9**, 570 (abstr.).

_____ (1969): X-ray data, optical anisotropism, and thermal stability of cobaltite, gersdorffite, and ullmannite. *Mineral. Mag.* **37**, 26-33.

_____ & Stephenson, N.C. (1968): The crystal structure of gersdorffite (III), a distorted and disordered pyrite structure. *Mineral. Mag.* **36**, 940-947.

Berry, L.G. & Thompson, R.M. (1962): X-ray powder data for ore minerals: the Peacock atlas. *Geol. Soc. Am., Mem.* **85**.

Béziat, D., Monchoux, P. & Tollon, F. (1996): Cobaltite–gersdorffite solid solution as a primary magmatic phase in spessartite, Lacaune area, Montagne Noire, France. *Can. Mineral.* **34**, 503-512.

Bragg, W.L. (1914): The analysis of crystals by the X-ray spectrometer. *Proc. R. Phys. Soc. London* **89A**, 468-489.

Buerger, M.J. (1932): The crystal structure of löllingite, $FeAs_2$. *Z. Kristallogr.* **62**, 165-187.

_____ (1934): The pyrite–marcasite relation. *Am. Mineral.* **19**, 37-61.

_____ (1936): The symmetry and crystal structure of the minerals of the arsenopyrite group. *Z. Kristallogr.* **95**, 83-113.

Cabri, L.J., Harris, D.C. & Weiser, T.W. (1996): Mineralogy and distribution of platinum-group mineral (PGM) placer deposits of the world. *Explor. Mining. Geol.* **5**, 73-167.

Craig, J.R. & Scott, S.D. (1982): Sulfide phase equilibria. *Rev. Mineral.* **1**, CS-1 to CS-110.

Ferguson, R.B. (1946): Unit cell of glaucodot. *Geol. Soc. Am., Bull.* **57**, 1193 (abstr.).

Fleet, M.E. (1972): The crystal structure of pararammelsbergite ($NiAs_2$). *Am. Mineral.* **57**, 1-9.

_____ (1982): Synthetic smythite and monoclinic Fe_3S_4. *Phys. Chem. Minerals* **8**, 241-246.

_____ & Burns, P.C. (1990): Structure and twinning of cobaltite. *Can. Mineral.* **28**, 719-723.

Fuess, H., Kratz, T., Töpel-Schadt, J. & Miehe, G. (1987): Crystal structure refinement and electron microscopy of arsenopyrite. *Z. Kristallogr.* **179**, 335-346.

Fukuoka, M. & Hirowatari, F. (1980): On minerals in the system Ni–Co–As–S from the bedded manganese ore deposits in the eastern part of Yamaguchi Prefecture; on the chemical composition of gersdorffite–cobaltite solid solution. *Sci. Rep. Fac. Sci., Kyushu Univ., Geology* **13**, 239-249.

Garrido, C.J & Bodinier, J.L. (1999): Diversity of mafic rocks in the Ronda Peridotite: evidence for pervasive melt/rock reaction during heating of subcontinental lithosphere by upwelling asthenosphere. *J. Petrol.* **40**, 729-754.

GERVILLA, F. (1998): Magmatic ores in Ronda and Beni Bousera peridotites: the combined role of melt/rock interaction and tectonic evolution. *Bull. Liaison, Soc. Fr. Minéral. Cristallogr.* **10**, 41.

_____ & LEBLANC, M. (1990): Magmatic ores in high-temperature alpine-type lherzolite massifs (Ronda, Spain, and Beni Bousera, Morocco). *Econ. Geol.* **85**, 112-132.

_____, _____, TORRES-RUIZ, J. & FENOLL HACH-ALÍ, P. (1996): Immiscibility between arsenide and sulfide melts – a mechanism for the concentration of noble metals. *Can. Mineral.* **34**, 485-502.

_____, PAPUNEN, H., KOJONEN, K. & JOHANSON, B. (1998): Platinum-, palladium- and gold-rich arsenide ores from the Kylmäkoski Ni–Cu deposit (Vammala Nickel Belt, SW Finland). *Mineral. Petrol.* **64**, 163-185.

GIESE, R.F., Jr. & KERR, P.F. (1965): The crystal structures of ordered and disordered cobaltite. *Am. Mineral.* **50**, 1002-1014.

HALL, S.R. & STEWART, J.M. (1973): The crystal structure of argentian pentlandite (Fe, Ni)$_8$AgS$_8$ compared with the refined structure of pentlandite (Fe,Ni)$_9$S$_8$. *Can. Mineral.* **12**, 169-177.

HEM, S.R. (1998): *The Ore Mineralogy of the Arroyo de la Cueva Deposits, Ronda Peridotite, South Spain.* Cand. Scient. thesis, Univ. of Copenhagen, Copenhagen, Denmark.

HULLIGER, F. (1968): Crystal chemistry of chalcogenides and pnictides of the transition elements. *Struct. Bonding* **4**, 83-229.

HUHMA, A. & HUHMA, M. (1970): Contributions to the geology and the geochemistry of the Outokumpu region. *Geol. Soc. Finland, Bull.* **42**, 57-88.

IOFFE, P.A., TSENEKHMAN, L.S., PARSIKOVA, L.N. & BOBKOVSK, A.G. (1985): The chemical state of the iron atoms in FeS_2, FeAsS, $FeAs_2$. *Russ. J. Inorg. Chem.* **30**, 1566-1568.

IXER, R.A., STANLEY, C.J. & VAUGHAN, D.J. (1979): Cobalt-, nickel- and iron-bearing sulpharsenides from the north of England. *Mineral. Mag.* **43**, 389-395.

KAIMAN, S. (1947): The crystal structure of rammelsbergite. *Univ. Toronto, Stud. Geol.*, **51**, 49-58.

KANEDA, H., TAKEUCHI, S. & SHOJI, T. (1986): Stability of pentlandite in the Fe–Ni–Co–S system. *Mineral. Deposita* **21**, 169-180.

KERESTEJIAN, T. (1984): Alloclasite–cobaltite paramorphic transformation in the ores of the Vatia deposit, west Balkan Mountain. *Geologica Balcanica* **14**, 73-78.

KINGSTON, P.W. (1971): On alloclasite, Co–Fe sulpharsenide. *Can. Mineral.* **10**, 838-846.

KLEMM, D.D. (1965): Synthesen und Analysen in den Dreiecksdiagrammen FeAsS–CoAsS–NiAsS und FeS_2–CoS_2–NiS_2. *Neues Jahrb. Mineral., Abh.* **103**, 205-255.

KNOP, O. & IBRAHIM, M.A. (1961): Chalcogenides of the transition elements. II. Existence of the π phase in the M_9S_8 section of the system Fe–Co–Ni–S. *Can. J. Chem.* **39**, 297-317.

KOJONEN, K. (1976): Experiments on synthetic pentlandite. *Neues Jahrb. Mineral., Abh.* **126**, 133-135.

KONTNY, A., DE WALL, H., SHARP, T.G. & PÓSFAI, M. (2000): Mineralogy and magnetic behaviour of pyrrhotite from a 260°C section at the KTB drilling site, Germany. *Am. Mineral.* **85**, 1416-1427.

KRETSCHMAR, U. & SCOTT, S.D. (1976): Phase relations involving arsenopyrite in the system Fe–As–S and their application. *Can. Mineral.* **14**, 364-386.

LAROUSSI, A., MOËLO, Y., YAMAN, S. & TOURAY, J.-C. (1992): Study of cobaltite and alloclasite in the Esendemir skarn-type ore deposit (Ulukisla–Nigde) by electron microprobe technique. *Turkish J. Earth Sci.* **1**, 57-61.

LINDQUIST, M., LUNDQUIST, D. & WESTGREN, A. (1936): The crystal structure of Co_9S_8 and of pentlandite (Fe,Ni)$_9$S$_8$. *Svensk Kemisk Tidskrift* **48**, 156-160.

MAKOVICKY, M., MAKOVICKY, E. & ROSE-HANSEN, J. (1985): Experimental studies on the solubility and distribution of platinum group elements in base-metal sulphides in platinum deposits. *In* Metallogeny of Basic and Ultrabasic Rocks (M.J. Gallagher, R.A. Ixer, C.R. Neary & H.M. Prichard, eds.). The Institution of Mining and Metallurgy, London, U.K. (415-425).

MAUREL, C. & PICOT, P. (1974): Stabilité de l'alloclasite et de la cobaltite dans le systèmes Co–As–S et Co–Ni–As–S. *Bull. Soc. fr. Minéral. Cristallogr.* **97**, 251-256.

MERKLE, R.K.W. & VON GRUENEWALDT, G. (1986): Compositional variation of Co-rich pentlandite; relation to the evolution of the upper zone of the western Bushweld Complex, South Africa. *Can. Mineral.* **24**, 529-546.

MORIMOTO, N. & CLARK, L.A. (1961): Arsenopyrite crystal-chemical relations. *Am. Mineral.* **46**, 1448-1469.

MPOSKOS, E. (1983): A mineralogical study of the Au–Ag–Bi–Te–Cu–Co–Ni–As–S ore mineralisation in Macedonia, Greece. *Chem. Erde*, **42**, 281-296.

NICKEL, E.H. (1968): Structural stability of minerals with the pyrite, marcasite arsenopyrite and löllingite structures. *Can. Mineral.* **9**, 311-321.

_____ (1970): The application of ligand-field concepts to an understanding of the structural stabilities and solid-solution limits of sulphides and related minerals. *Chem. Geol.* **5**, 233-241.

OKAMOTO, H. & MASSALSKI, T.B. (1983): The Au–Bi (gold–bismuth) system. *Bull. Alloy Phase Diagrams* **4**, 401-407.

PEARSON, A.D. & BUERGER, M.J. (1956): Confirmation of the crystal structure of pentlandite. *Am. Mineral.* **41**, 804-805.

PETRUK, W., HARRIS, D.C. & STEWART, J.M. (1969): Langisite, a new mineral, and the rare minerals cobalt pentlandite, siegenite, parkerite and bravoite from the Langis mine, Cobalt–Gowganda area, Ontario. *Can. Mineral.* **9**, 597-616.

_____, _____ & _____ (1971): Characteristics of the arsenides, sulpharsenides and antimonides. *Can. Mineral.* **11**, 150-186.

POLUSHKINA, A.P. & SIDORENKO, G.A. (1963): A structural variety of cobaltite. *Dokl. Acad. Sci. USSR* **153**, 167-170.

PÓSFAI, M., SHARP, T.G. & KONTNY, A. (2000): Pyrrhotite varieties from the 9.1. km deep borehole of the KTB project. *Am. Mineral.* **85**, 1406-1415.

PRIEM, H.N.A., BOELRIJK, N.A.I.M., HEBEDA, E.H., OEN, I.S., VERDUMEN, E.A.T. & VERSCHURE, R.H. (1979): Isotopic dating of the ultramafic masses in the Serrania de Ronda, southern Spain. *Contrib. Mineral. Petrol.* **70,** 103-109.

RADCLIFFE, D. & BERRY, L.G. (1968): The safflorite–löllingite solid solution series. *Am. Mineral.* **53**, 1856-1881.

_____ & _____ (1971): Clinosafflorite: a monoclinic polymorph of safflorite. *Can. Mineral.* **10**, 877-881.

RAJAMANI, V. & PREWITT, C.T. (1973): Crystal chemistry of natural pentlandites. *Can. Mineral.* **12**, 178-187.

REISBERG, L., ZINDLER, A. & JAGOUTZ, E. (1989): Further Sr and Nd isotopic results from peridotites of the Ronda ultramafic complex. *Earth. Planet. Sci. Lett.* **96**, 161-180.

RILEY, J.F. (1977): The pentlandite group (Fe, Ni,Co)$_9$S$_8$: new data and an appraisal of structure–composition relationships. *Mineral. Mag.* **41**, 345-349.

SCOTT, J.D. & NOWACKI, W. (1976): The crystal structure of alloclasite, CoAsS, and the alloclasite–cobaltite transformation. *Can. Mineral.* **14**, 561-566.

SCOTT, S.D. & KISSIN, S.A. (1973): Sphalerite composition in the Zn–Fe–S system below 300°C. *Econ. Geol.* **68**, 475-479.

SHARP, Z.D., ESSENE, E.J. & KELLY, W.C. (1985): A re-examination of the arsenopyrite geothermometer: pressure considerations and applications to natural assemblages. *Can. Mineral.* **23**, 517-534.

SUGAKI, A. & KITAKAZE, A. (1998): High form of pentlandite and its thermal stability. *Am. Mineral.* **83**, 133-140.

SUNDBLAD, K., ZACHRISSON, E., SMEDS, S.-A., BERGLUND, S. & ÅLINDER, C. (1984): Sphalerite geobarometry and arsenopyrite geothermometry applied to metamorphosed sulfide ores in the Swedish Caledonides. *Econ. Geol.* **79**, 1660-1668.

TAYLOR, L.A. & WILLIAMS, K.L. (1972): Smythite (Fe, Ni)$_9$S$_{11}$ – a redefinition. *Am. Mineral.* **57**, 1571-1577.

TOSSELL, J.A. (1984): A reinterpretation of the electronic structures of FeAs$_2$ and related minerals. *Phys. Chem. Minerals* **11**, 75-80.

_____, VAUGHAN, D.J. & BURDETT, J.K. (1981): Pyrite, marcasite, and arsenopyrite type minerals; crystal chemical and structural principles. *Phys. Chem. Minerals* **7**, 177-184.

TSUKIMURA, K., NAKAZAWA, H., ENDO, T. & FUKUNAGA, O. (1992): Cation distribution in pentlandites (Fe, Ni)$_9$S$_8$; dependence on pressure and temperature and kinetics of the cation exchange reaction. *Phys. Chem. Minerals* **19**, 203-212.

VAN DER WAL, D. & BODINIER, J.L. (1996): Origin of the recrystallization front in the Ronda peridotite by km-scale pervasive porous melt flow. *Contrib. Mineral. Petrol.* **122**, 387-405.

VINOGRADOVA, R.A., ULJANOV, A.A., KOROTAEVA, N.N. & OBRAZTSOV, V.V. (1994): Selenium bearing sulpharsenides of the cobaltite–gersdorffite series from deposits of Bou-Azzer district (Morocco). *Zap. Vser. Mineral. Obshchest.* **123**(5), 64-69 (in Russ.).

WOOD, B.J.& STRENS, R.G.J. (1979): Diffuse reflectance spectra and optical properties of some sulphides and related minerals. *Mineral. Mag.* **43**, 509-518.

ZECK, H.P., ALBAT, F., HANSEN, B.T., TORRES-ROLDÁN, R.L., GARCÍA-CASCO, A. & MARTÍN-ALGARRA, A. (1989): A 21±2 Ma age for the termination of the ductile Alpine deformation in the internal zone of the Betic Cordilleras, south Spain. *Tectonophys.* **169**, 215-220.

ZINDLER, A., STAUDIGEL, H., HART, S.R., ENDRES, R. & GOLDSTEIN, S. (1983): Nd and Sr isotopic study of a mafic layer from the Ronda ultramafic complex. *Nature* **304**, 226-230.

Received February 29, 2000, revised manuscript accepted March 16, 2001.